3D Simulation of Active thin Structures in a Viscous Fluid and Application to Mucociliary Transport

Astrid Decoene, Sébastien Martin, Chabane Méziane

Math. Model. Nat. Phenom. 19 (2024) 12
https://doi.org/10.1051/mmnp/2024010

Mathematical Modelling of Natural Phenomena
www.mmnp-journal.org

3D SIMULATION OF ACTIVE THIN STRUCTURES IN A VISCOUS FLUID AND APPLICATION TO MUCOCILIARY TRANSPORT

Astrid Decoene[1], Sébastien Martin[2,*] and Chabane Méziane[3]

Abstract. We propose a hierarchy of mathematical models for the numerical simulation of active thin structures in a viscous fluid and its application to mucociliary clearance. Our aim is to simulate large forests of cilia and analyze the collective dynamics arising in the flow, as well as their impact on the efficiency of the mucus transport. In a 3D model we describe the cilia individually and study their joint actions on the fluid. The model is built upon a 3D Stokes problem with singular source terms that represent the action of the 1D cilia on the fluid, including the influence of the background flow (making the problem nonlocal). Surface tension between the periciliary layer and the mucus is taken into account. From the 3D model we also derive a 1D space averaged model, describing the dynamics of the mean velocity of the mucus that is propelled by the cilia, hence allowing lower computational costs and still providing useful characterization of the efficiency of the transport. Mathematical properties of the models (existence and uniqueness of solutions in suitable functional spaces) are analyzed. Numerical simulations highlight the influence of critical parameters on the efficiency of the mucociliary transport in the case of dense forests of cilia.

Mathematics Subject Classification. 76D07, 92C35, 68U20.

Received October 27, 2023. Accepted May 17, 2024.

1. Introduction

The present work deals with the mathematical modeling and the numerical simulation of active thin structures in a viscous fluid and its application to mucociliary clearance. The human lung is protected against dehydration and inhaled particles, like dust or allergens, by a thin liquid layer lining the interior of the airways. This airway surface liquid is a bilayer composed of mucus, a visco-elastic fluid secreted by the respiratory epithelium [1], and a thin fluid layer known as the periciliary liquid [2], commonly called PCL. Preserving the lung from inhaled impurities is necessary, since they could obstruct the bronchi and limit the exchange area for oxygen and carbon dioxide. Mucus traps aspirated particles and is then itself evacuated from the lung by the action of numerous cilia lining the lung bronchi. Other factors that help drain mucus in the bronchial tree are cough and forced breathing [3]. Under pathological conditions, mucus characteristics and mucociliary clearance efficiency can be

Keywords and phrases: Mucociliary transport, nonlocal Stokes problem, singular source term.

[1] Université de Bordeaux, Institut de Mathématiques de Bordeaux (CNRS-UMR 5251), 351 cours de la Libération, 33405 Talence, France.
[2] Université Paris Cité, Laboratoire MAP5 (CNRS-UMR 8145), 45 rue des Saints-Pères, 75270 Paris cedex 06, France.
[3] Université Paris-Saclay, Laboratoire de Mathématiques d'Orsay (CNRS-UMR 8628), Bâtiment 307, rue Michel Magat, Faculté des Sciences d'Orsay, 91405 Orsay cedex, France.

* Corresponding author: sebastien.martin@u-paris.fr

altered. For example, due to a modification of the viscosity of the mucus or a degradation of cilia, ciliary motion can become ineffective, inducing mucus stasis that often leads to infections.

Active research has been devoted to the study of the motion of bronchial cilia since the pioneering work by Lucas [4]. Cilia are very slender structures whose length is about 6 μm and radius is 0.1 μm, and they are fixed on the epithelial cells in the bronchi. They beat in the periciliary layer, where viscosity is much lower than in the mucus, at an average frequency of 15 Hz depending on the characteristics of the environment. A detailed description of the mechanism of motility has been given by Gibbons in [5] and more recently in [6–8]. Each beat of a cilium can be divided into two phases, a recovery stroke and an effective stroke, during which the motion is not symmetric under time reversal. In fact, since mucus and PCL are viscous fluids at the scale of a cilium, a reversible movement of the cilium would not permit the mucus to be transported [9]. According to Sanderson and Dirksen [10], the effective stroke is two or three times faster than the recovery stroke, and cilia may penetrate the overlying mucus during the faster phase. Cilia that propel mucus coordinate into a metachronal wave, which wavelength is of the order of a hundred of cilia, that is around 30 μm, and that propagates in the opposite direction of mucus transport. It is believed that coordination of the beating into a metachronal wave arises during the recovery stroke and is due to hydrodynamic interactions between the cilia [11]. Changes in the viscosity of the medium, in the length or in the spacing of the cilia may therefore have a deep influence on the characteristics of the metachronal wave.

The complexity of the process is high (high amount of cilia, three layers if we consider air that is driven in the bronchus, several interfaces, several scales, *etc.*) and only a few data are available. Although a wide variety of works can be found in the literature about mucociliary clearance, the numerical simulation remains at present time a challenge.

Some authors have developed models in which the action of cilia is represented *via* a prescribed velocity at the bottom of the mucus layer, like for instance in [12], where a numerical investigation of the interaction between respiratory mucus motion and air circulation is presented. Using the same approach, Mitran proposes in [13] a multiscale model to study the effect of airflow shear forces, as exerted by tidal breathing and cough, upon clearance, and Mauroy and coauthors investigate in [14] the role of the geometry of the airway tree on clearance. These works present interesting multiscale approaches of the process but they do not allow to investigate details of the role of ciliary motion.

Other authors use a continuum representation of the airway surface liquid as a traction layer, with a continuous distribution of forces. In [15], for instance, Smith and coauthors replace the forest of cilia by an active porous medium in which the cilia are modeled by a volumic resistive force directly dependent on the local velocity of the cilia. They consider a three-layer fluid in dimension 2: a Maxwell fluid for the mucus, a Newtonian fluid for the periciliary layer and a layer of transition. Kurbatova and coauthors use the same model in [16] in order to estimate mucociliary velocity in different generations of the lung, adding influx terms from previous generations and production of mucus. In [17] Choudhury and coauthors replace the forest of cilia by a Navier-slip boundary condition derived in [18] which allows for a continuum description of the mucus film (considered as viscolelastic, not purely viscous).

A very different approach consists in representing the cilia individually, either by prescribing their beating or by modeling in some way their internal activity. Several authors have worked on models for the internal activity of cilia, in order for instance to investigate the emergence of ciliary metachronism [19–23]. In [20] for instance, Dillon and coauthors used a discrete representation of the internal structures of cilia and a curvature control mechanism for their activity, and solved the interaction of these structures with the fluid (PCL and mucus) in 2D using the immersed boundary method. Sedaghat and coauthors use hybrid finite difference-lattice Boltzmann-method combined with immersed boundary method, in 2D, to investigate the additional effect of viscoelasticity in 2D [24] and in 3D [25]. Mitran [26] proposed the most complete model for the internal mechanism of bronchial cilia, with a detailed description of the internal microtubule structures in 3D using thin-wall beams and spring elements to model nexin links. Activity was modelled through a forces scenario exerted between adjacent microtubules. The fluid-structure interaction was solved using finite elements for the structure and finite volumes for fluid. He simulated the configuration of up to 256 cilia in a row, bringing evidence for a hydrodynamic origin to observed ciliary synchronization. However, the computational effort is such that no

parametric study could be made. Recent works have proposed models based on a sliding regulation mechanism for dynein activity proposed in [27]. Cilia movement is modeled with 1D elastic equations and the fluid-structure problem is solved using the slender body theory. These works have allowed to reproduce typical spontaneous oscillations observed in cilia [28] as well as synchronization resulting from hydrodynamical interactions [29, 30].

Nevertheless, how the internal ciliary engine affects the ciliary beat form is still not completely understood, and its modelling induces heavy additional computational effort. That is why many works focus on the flow fields produced by cilia with given beat pattern and frequency. Due to their slenderness, the action of individual cilia can be represented by a centerline distribution of forces, following the slender body theory (see for instance [31], or for a rigorous asymptotic analysis [32]). This idea was initially developed in studies such as Liron and Mochon [33] and Fulford and Blake [34], and then further developed in other works [22]. The distribution of point forces is derived from the prescribed beat pattern either using an asymptotic formula, as in [34], or by prescribing the velocity at the surface of each cilium as in [33] and [35], leading to the resolution of an integral equation. The different works based on this idea can be distinguished by the way the force distribution is computed, but also by the use of particular singular solutions adapted to the conditions at the boundaries of the domain. They have obtained estimates of the mean field velocity in both the periciliary layer and the mucous layer (both liquids being assumed to have Newtonian fluid properties), but the profiles are time- and space-averaged. Besides, no penetration of the cilia into the mucus layer is taken into account. They show that the mean field velocity is very small in the lower part of the periciliary layer and increases very quickly close to the mucus layer. In [36] the authors used a similar model in 2D allowing to investigate non-averaged velocity profiles both in the PCL and in the mucus; a parametric study was made, showing the impact of changing the viscosity ratio or the length of cilia. In particular, they show that the velocity of mucus decreases when its viscosity increases, what they explain *via* the fact that viscous forces between the mucus and the PCL increase. In [37] cilia are also modeled by thin structures whose deformations are prescribed. However the computations are 3-dimensional and the numerical method is different : the equality of the fluid and solid velocities on the fluid-structure interface is imposed with the immersed boundary method. In addition, the action of the fluid on the structure is partially taken into account, modeled by a damping term that changes the intensity of the velocity of the structures. The authors investigate synchronization of cilia through hydrodynamic interactions, but the velocity profiles inside the layers are not analyzed.

Some works consider a 3-dimensional representation of each cilium with prescribed movement. Chatelin and coauthors [38], for instance, proposed a 3-dimensional model where the viscosity is the solution of a convection-diffusion equation of mucin proteins. The movement of the cilia is prescribed and the effects of the cilia on the fluid are treated by an efficient fictitious domain method. However the amount of cilia in simulations remains limited, due to the high computational cost induced by the representation of the structure's thickness. In [39], the authors modeled in two-dimension the viscosity as the solution of a reaction-advection-diffusion equation depending on the temperature, but the model for the flow is very simplified. To the best of our knowledge, in the other works which consider a variable viscosity, the viscosity is defined constant by part.

This work focuses on a model that allows to efficiently simulate a large amount of active thin structures and perform a parametric study to investigate the impact of different parameters on mucus velocity. The complexity of the phenomenon leads us to consider several restrictive assumptions. On the one hand, we have chosen to work in the case of a prescribed movement of the structures, in the asymptotic limit of infinite slenderness: we thus represent the slender bodies as 1D curves immersed in a 3D viscous flow. The action of the structures on the fluid is represented through a Dirac distribution of forces along the 1D curve. Retroaction of the fluid on the structures is not taken into account. On the other hand, although mucus is a viscoelastic fluid, its relaxation time is long with respect to the cilia beating cycle. It is thus reasonable to model it as a Newtonian viscous fluid. And since both mucus and the PCL are viscous at the scale of the cilia, we solve the Stokes equations in both layers. The significant difference in viscosity is taken into account through a bi-fluid model with a fixed and flat interface, consistently to experimental observations. The presence of air above the mucus layer is taken into account through a boundary condition, airways are not represented in our simulations. A bottom-up approach is developped: i) at the cilia individual scale, we use equations of motion for 3D Stokes flow to which we associate the cilia individually and solve the action of each of them on the fluid. ii) at an averaged scale, we derive a

1D model that describes how the ciliary activity governs the mean axial velocity of the fluid (which is directly related to the efficiency of the mucociliary transport), with a computational cost that is considerably lowered. A rigorous mathematical framework is presented for both problems, including well-posedness in suitable functional spaces. Additionally, we use a finite element method to solve both problems: the method is still well-defined in the presence of the singular source term and the rigorous error analysis has been performed in [40] (the FEM is still proven to be converging, with a convergence rate that is locally slowed down). The models and numerical methods allow us to simulate the action of very large forests of cilia on the flow, and investigate the impact of some parameters on the mucociliary efficiency. They can contribute to a better understanding of mechanisms involved in mucociliary clearance, in the perspective of analyzing the collective dynamics arising in the flow, as well as their impact on the efficiency of the mucus transport.

This paper is organized as follows: in Section 1 we describe the model developed for the fluid-cilia interaction, and in Section 2 we discuss the mathematical properties of the resulting equations, *i.e.* a nonlocal Stokes system with a singular right-hand side. Section 3 is devoted to the numerical method developed in order to retrieve the optimal order of the finite element method applied to these equations. The last section concerns the application of this model to the simulation of the mucociliary transport and the presentation of numerical results in a reference configuration along with an investigation of critical parameters for the mucociliary efficiency.

2. Three-dimensional modelling

We are interested in modelling the interaction of active cilia with a viscous flow in the context of mucociliary transport. Bronchial cilia are attached to the bronchial walls and immersed in a bilayer composed of a first thin liquid layer called the periciliary liquid (PCL), adjacent to the walls, and a second layer composed of mucus (see Fig. 1). They essentially beat inside the PCL, but eventually penetrate the mucus layer during a short part of their periodic movement. At the top of the bilayer, mucus is in contact with the air flowing inside the bronchi. Since the aim of this work is to simulate dense suspensions of active cilia, we are concerned with limiting the computational cost related to the problem, while trying to keep assumptions minimal.

An essential feature of our problem is that cilia are slender bodies that beat very quickly in the viscous fluid. In the case of bronchial cilia, the ratio between their cross-sectional radius and their length is $\frac{r}{L} \sim \frac{0.1}{6}$, and their beating frequency is about $f = 15$ Hz. Representing each cilium as a three-dimensional body immersed in the fluid domain involves a considerable computational effort to represent the fluid-body interface. An option in order to reduce this cost can be to use a fictitious domain approach (see for instance [38]). However, we have chosen to take advantage of the geometry of the structure and work in the asymptotic of infinite slenderness, that is when the ratio between the thickness and the length of the structure $\epsilon = \frac{r}{L}$ vanishes. Keeping the force exerted by each section of the body constant when ϵ vanishes allows to conserve the action of the cilium on the fluid, while the velocity of the fluid becomes infinite at the centerline of the slender body. Our model thus consists of the Stokes equations governing the dynamics of a viscous fluid, with in the source term a line distribution of forces along a 1D curve representing the thin structures. For an analysis of the convergence of the solution to the full problem, that means with a volumic distribution of the hydrodynamic force on the 3D structure, to the solution of the asymptotic model when ϵ vanishes, we refer the reader to [41].

As for the activity of the cilia, a complete model would consist in a mechanical model for the structure coupled to the fluid equations, so that both the action of the structure on the fluid and the retroaction of the fluid on the structure are taken into account. However, modeling the mechanics of active thin structures like the bronchial cilia for instance is a difficult task, since the underlying internal dynamics are not well understood. Besides, since the solution of the Stokes problem with a line Dirac distribution is singular, our model does not allow to compute the velocity of the structure in a straightforward way in order to retrieve its movement. That is why in this work, we do not address the problem of the construction of the mechanical model, and we consider that the movement of each cilium is given. The resulting model is therefore "one-way", in the sense that it only aims at reproducing the effects of the active structures on the fluid and neglects the retroaction of the fluid on the structures.

On the other hand, experiments show that the PCL-mucus interface does not evolve in time, presumably due to surface tension. We will take into account surface tension and enforce the interface to be constant in time. In addition we will assume both the PCL-mucus and the mucus-air interfaces to be at all times parallel to the bronchial walls.

Parametrization of a cilium and of a forest of cilia

We use the parametrization established by Fulford and Blake in [42], based on the Fourier series decomposition of the beat of one cilium of cultured rabbit tracheal epithelium described in [43]. The authors also proposed an extension of the parametrization to the movement of a whole forest of cilia, *via* two parameters that represent respectively the distance between two cilia and the wavelength of the metachronal wave. It is based on the assumption that the metachronal wave propagates in the direction of the cilia beat, although experiments show that some activity is also propagated in the transversal direction. However this approximation is classical and experiments [44] show that increasing viscosity causes the metachronal wave to become more and more orthoplectic (*i.e.* in the direction of mucociliary transport). In the simulations presented in this paper, this assumption has also been made, but the model allows to prescribe a metachronal wave with arbitrary direction.

Let us start with the parametrization of the movement of a single cilium. A cilium is assumed to evolve in a $(x-z)$ plane: at each time t the cilium is represented by the truncated Fourier series of the parametric curve

$$\boldsymbol{\xi}^{2D}(s,t) = \begin{pmatrix} \xi_x^{2D}(s,t) \\ \xi_z^{2D}(s,t) \end{pmatrix} = L\left[\frac{1}{2}\mathbf{a}_0(s) + \sum_{n=1}^{6} \mathbf{a}_n(s)\cos(2n\pi f t) + \mathbf{b}_n(s)\sin(2n\pi f t)\right],$$

where $s \in [0,1]$ measures arclength from the base of the cilium, L and f are respectively the length and the beat frequency of the cilium. The Fourier coefficients $\mathbf{a}_n$, $\mathbf{b}_n$ are vector quantities, which are approximated by the following 3-degree polynomial functions

$$\mathbf{a}_n(s) = \sum_{k=1}^{3} \mathbf{a}_{n,k} s^k \text{ and } \mathbf{b}_n(s) = \sum_{k=1}^{3} \mathbf{b}_{n,k} s^k$$

where $\mathbf{a}_{n,k}$ and $\mathbf{b}_{n,k}$ are constant vectors of $\mathbb{R}^2$, given in Table 1.

Figure 1 shows the beat of a cilium obtained using this parametrization and allows to observe a good correspondance with the description made by Sanderson and Sleigh in [43]. Let us note that the cilium crosses the interface between the mucus and the peryciliary layer (PCL) only during the effective stroke and not during the recovery stroke. This feature is known to be important in order to guarantee an efficient mucus transport.

The extension to a 3D setting is natural: assume that the cilium evolves in the $(x-z)$ plane at $y = y^{(0)}$, we define

$$\boldsymbol{\xi}(s,t) = \begin{pmatrix} \xi_x^{2D}(s,t) \\ y^{(0)} \\ \xi_z^{2D}(s,t) \end{pmatrix}.$$

The parametrisation of a whole forest of cilia given in [42] depends on two important parameters : the space ℓ_0 between two cilia (in each direction) and the wavelength λ of the metachronal wave. More precisely, in order to model a forest of $n_x \times n_y$ cilia, with n_x (respectively n_y) the number of cilia in the direction x (respectively the direction y), the cilium (i,j), where $i \in [\![1, n_x]\!]$ and $j \in [\![1, n_y]\!]$, is parametrized by the curve

$$\boldsymbol{\xi}^{(ij)}(s,t) = i\ell_x^0 \mathbf{e}_x + j\ell_y^0 \mathbf{e}_y + \boldsymbol{\xi}\left(s, \frac{i\ell_x^0}{f\lambda} + t\right),$$

TABLE 1. Fourier-least squares coefficients for the cilia beat pattern. The upper and lower numbers in each entry correspond to the x and z components respectively, the y component is always zero.

	$\mathbf{a}_{n,k}$						
	$n=0$	$n=1$	$n=2$	$n=3$	$n=4$	$n=5$	$n=6$
$k=1$	−0.449	0.130	−0.169	0.063	−0.050	−0.040	−0.068
	2.076	−0.003	0.054	0.007	0.026	0.022	0.010
$k=2$	−0.072	−1.502	0.260	−0.123	0.011	−0.009	0.196
	−1.074	−0.230	−0.305	−0.180	−0.069	0.001	−0.080
$k=3$	0.658	0.793	−0.251	0.049	0.009	0.023	−0.111
	0.381	0.331	0.193	0.082	0.029	0.002	0.048

	$\mathbf{b}_{n,k}$					
	$n=1$	$n=2$	$n=3$	$n=4$	$n=5$	$n=6$
$k=1$	−0.030	−0.093	0.037	0.062	0.016	−0.065
	0.080	−0.044	−0.017	0.052	0.007	0.051
$k=2$	1.285	−0.036	−0.244	−0.093	−0.137	0.095
	−0.298	0.513	0.004	−0.222	0.035	−0.128
$k=3$	−1.034	0.050	0.143	0.043	0.098	−0.054
	0.210	−0.367	0.009	0.120	−0.024	0.102

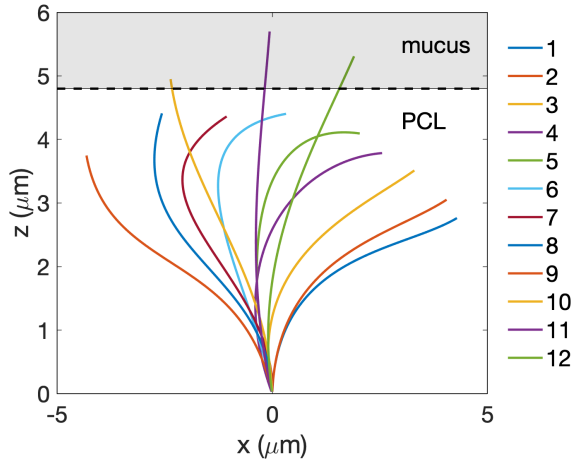

FIGURE 1. Traces of a cilium during one period of its beat with a PCL-mucus interface at $z = 4.8\,\mu\text{m}$. Description made by Sanderson and Sleigh [42, 43].

where $s \in [0,1]$. Let us note the phase shift $\varphi_i = i\ell_x^0/f\lambda$ in x (and only in x, as there is no phase shift not in y) which the metachronal wave comes from. We have drawn in Figure 2 a section of the forest in the direction x. The propagation of the metachronal wave (to the left on the picture) is in the opposite direction of mucus transport (to the right). Figure 3 shows a forest in 3D as we model it in the simulations, with values of the cilia spacings ℓ_x^0 and ℓ_y^0 that have been voluntarily increased for the sake of clarity.

Distribution of the forces exerted by the cilia on the fluid: the slender body theory

Since we work with a given movement of the cilia, defined by the parametrization introduced previously, we need to deduce the distribution of forces induced by this movement on the fluid. For that purpose, we use the

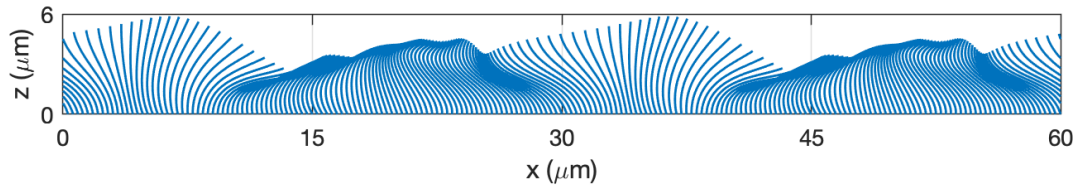

FIGURE 2. Parametrization of a dense forest of cilia: section of a forest with the parametrization established by Fulford and Blake [42] over two metachronal waves length.

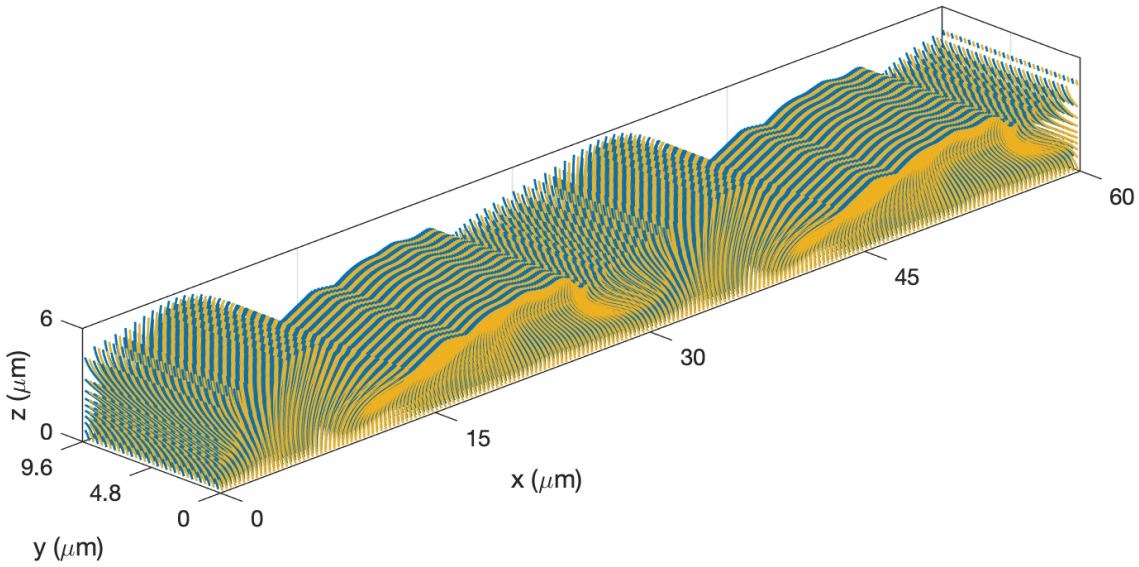

FIGURE 3. Dense forest of cilia with the parametrization established by Fulford and Blake [42] over two metachronal waves length. Ciliary spacing is 0.3 µm in both axial and azimuthal directions (hence 200×32 cilia are represented here).

so-called slender-body theory, based on asymptotic expansions when the ratio ϵ between the thickness and the length of the body vanishes. Cox [31] established an asymptotic expansion of the force at each point of the slender-body. If

$$s \mapsto \boldsymbol{\xi}(s,t)$$

is a parametrization of the position of the body at time t in curvilinear coordinates, the expression of the force at the point of curvilinear abscissa s is

$$\hat{\mathbf{f}}(s,t) := \frac{2\pi\mu}{\ln(L/r)} \left(2\mathbb{I}_3 - \frac{\partial_s\boldsymbol{\xi}(s,t) \otimes \partial_s\boldsymbol{\xi}(s,t)}{\|\partial_s\boldsymbol{\xi}(s,t)\|^2} \right) (\hat{\mathbf{u}}_{\text{cil.}}(s,t) - \mathbf{u}_{\text{bg}}) + O\left(\frac{1}{(\ln(L/r))^2} \right),$$

where $\hat{\mathbf{u}}_{\text{cil.}}(s,t) := \partial_t\boldsymbol{\xi}(s,t)$ denotes the local velocity of the slender body at curvilinear abscissa s and time t, and $\mathbf{u}_{\text{bg}}$ denotes the background flow (*i.e.* the velocity of the fluid in the absence of the structure). This relation has been established in [31] by confronting two different approaches:

1. the inner expansion consists in studying the fluid velocity near the slender body, which is thus seen as an infinite cylinder. The corresponding regime is L tends to infinity while a remains constant.

2. the outer expansion considers the flow far from the slender body seen as a zero-thickness body, which corresponds to the regime a goes to zero while L remains constant.

We apply the slender body theory as presented previously to compute the distribution of forces applied by each cilium on the fluid, and for the sake of more simple notations, we define

$$\hat{\mathbb{M}}(s,t) := \frac{2\pi\mu}{\ln(L/r)}\left(2\mathbb{I}_3 - \frac{\partial_s\boldsymbol{\xi}(s,t)\otimes\partial_s\boldsymbol{\xi}(s,t)}{\|\partial_s\boldsymbol{\xi}(s,t)\|^2}\right),$$

so that the slender body theory at main order relates the hydrodynamical force exerted by a single cilium to the ciliary dynamics by

$$\hat{\mathbf{f}}(s,t) = \hat{\mathbb{M}}(s,t)\cdot\left(\hat{\mathbf{u}}_{\text{cil.}}(s,t) - \hat{\mathbf{u}}_{\text{bg}}(s,t)\right), \tag{2.1}$$

Remark 2.1. In the presence of several cilia, the background flow $\mathbf{u}_{\text{bg}}$ takes into account the disturbance flow caused by adjacent cilia. The term involving the background flow then models how the collective dynamics due to all cilia damps/increases the action of each cilium over the fluid.

Remark 2.2. In order to fix ideas, it may be convenient to change the curvilinear coordinates into the 3D coordinates describing the cilia. Therefore we may use the following change of variables:

$$\mathbf{f}(\boldsymbol{\xi}(s,t);t) = \hat{\mathbf{f}}(s,t).$$

Remark 2.3. It is worthwhile noticing that assumptions on the cilia patterns (which evolve in the $(x-z)$ plane) lead to some simplifications: in particular $\partial_s\xi_y = 0$ so that

$$\partial_s\boldsymbol{\xi}\otimes\partial_s\boldsymbol{\xi} = \begin{pmatrix} |\partial_s\xi_x|^2 & 0 & \partial_s\xi_x\partial_s\xi_z \\ 0 & 0 & 0 \\ \partial_s\xi_x\partial_s\xi_z & 0 & |\partial_s\xi_z|^2 \end{pmatrix}.$$

As a consequence, if we assume that $\hat{u}_{\text{bg},y} = 0$ (which is a reasonable assumption, that will be discussed in Asm. 2.4) and since $\hat{u}_{\text{cil.},y} = \partial_t\xi_y = 0$, the second component of the force field is null, namely

$$\hat{f}_y(s,t) = 0.$$

Fundamental equations in 3D

We consider $(\mathbf{e}_x,\mathbf{e}_y,\mathbf{e}_z)$ an orthonormal basis in $\mathbb{R}^3$ and a domain $\Omega\subset\mathbb{R}^3$ defined as

$$\Omega = \{\mathbf{x} = (x,y,z)\in\mathbb{R}^3, x/L_x\in\mathbb{T},\ y/L_y\in\mathbb{T}, z\in(0,L_z)\}.$$

In order to capture the main phenomenological aspects, we set $L_x = \lambda$ corresponding to the length of the metachronal wave: this ensures the periodicity of the ciliary beat patterns in Ω. Moreover as the cilia evolve in the $(x-z)$ plane, most phenomena in the y direction can be neglected. Thus the domain is L_x-periodic in x, L_y-periodic in y and we denote the boundaries: $\Gamma_\downarrow = \{z=0\}$ is the lower boundary to which the cilia are fixed. $\Gamma_\uparrow = \{z=L_z\}$ is the upper boundary that corresponds to the top of the mucus layer. The fluid domain divides into two areas: the PCL, occupied by a fluid of viscosity μ_1, is the subdomain $\{z<H\}$; the mucus, occupied by a fluid of viscosity $\mu_2>\mu_1$ is the subdomain $\{z>H\}$. In this context, we define

$$\mu(z) = \begin{cases} \mu_1 & \text{if } z<H, \\ \mu_2 & \text{if } z>H. \end{cases}$$

The interface between the PCL and the mucus is located at $\Gamma_* = \{z = H\}$. We consider a list of thin structures (i, j), where $i \in [\![1, n_x]\!]$ and $j \in [\![1, n_y]\!]$, immersed in Ω and fixed to the bottom of the domain $\Gamma_\downarrow$. We denote by $s \mapsto \boldsymbol{\xi}^{(ij)}(s, t)$ the parametrization of their motion at time t. Note that in the context of a viscous flow governed by Stokes equations, the system is instantaneous and time only plays the role of a parameter (therefore it will be regularly omitted when no ambiguity emerges from the equations). The resulting mathematical problem consists in finding a velocity field $\mathbf{x} \mapsto \mathbf{u}(\mathbf{x})$, a pressure field $\mathbf{x} \mapsto p(\mathbf{x})$, and a surface tension $(x, y) \mapsto \gamma(x, y)$ such that $(\mathbf{u}, p, \gamma)$ are periodic in x and y and

$$\left\{\begin{array}{rcll} -\mathrm{div}(\mu\nabla\mathbf{u}) + \nabla p + \gamma\mathbf{e}_z\delta_{\Gamma_*} &=& \displaystyle\sum_{i,j} \mathbf{f}_{ij}[\mathbf{u}]\,\delta_{\Gamma_{ij}} & \text{in } \Omega, \\ \mathrm{div}(\mathbf{u}) &=& 0 & \text{in } \Omega, \\ [(\mu\nabla\mathbf{u} - p\mathbb{I})\cdot\mathbf{n}]\cdot\mathbf{t} &=& 0 & \text{on } \Gamma_\uparrow, \\ \mathbf{u}\cdot\mathbf{n} &=& 0 & \text{on } \Gamma_\uparrow \cup \Gamma_*, \\ \mathbf{u} &=& 0 & \text{on } \Gamma_\downarrow. \end{array}\right. \tag{2.2}$$

Here Γ_{ij} denotes the 1D curve describing the centerline of the (i, j)-th structure, and $\mathbf{f}_{ij}[\mathbf{u}](\cdot, t)$ is the force distribution it exerts by the structure at time t on the fluid (it has been partially described previously, through the slender body theory and we recall that it may depend on the solution $\mathbf{u}$ because of the influence of the background flow - as this will be detailed further). Let us argue on the condition $u_z = 0$ on the PCL-mucus interface Γ_*: it is noticed in experiments that the interface does not evolve in time, presumably due to surface tension. From the mathematical point of view, this constraint is imposed by duality: for that purpose we introduce the surface tension γ (to be determined) located at the interface, which serves as a Lagrange multiplier for the constraint $u_z = 0$ on Γ_*.

At the bottom we impose a no-slip boundary condition ($\mathbf{u} = 0$) on $\Gamma_\downarrow$, while at the top of the box we prescribe so-called free-slip conditions on $\Gamma_\uparrow$: $\mathbf{u}\cdot\mathbf{n} = 0$ is the kinematic condition, whereas $[(\mu\nabla\mathbf{u} - p\mathbb{I})\cdot\mathbf{n}]\cdot\mathbf{t} = 0$ is the dynamic condition. Here $\mathbf{n}$ is the normal outward unit vector, $\mathbf{t}$ the tangential unit vector associated to the interface. Prescribing this kinematic condition means that we assume that the particles of fluid do not cross the mucus/air interface, so that this interface remains flat and constant during the whole simulation, which is a reasonable assumption with regard to the experimental results available. The dynamic condition implies that we neglect friction of the air layer. More complex boundary conditions could be considered in order to take into account the effect of the airflow on the mucus layer, as for instance a prescribed shear stress (see for instance [14] and [13]). Finally, the box we consider is seen as a window focused on a part of a bronchus, and mucociliary transport goes on outside this box. Therefore it is natural to impose biperiodic boundary conditions in both directions (this requires that the computation domain extends so that a full metachronal wavelength is taken into account).

Source terms

Let us come back to the term $\mathbf{f}_{ij}[\mathbf{u}]$ that describes the force distribution the cilium exerts on the fluid. As previously mentioned, the definition relies on equation (2.1) but the background flow velocity needs to be specified. Because of the configuration of the cilia forest, we assume the following:

Assumption 2.4. We denote the fluid flow by $\mathbf{u} = (u_x, u_y, u_z)$ and we approximate the background flow velocity defined over Ω by

$$\mathbf{u}_{\mathrm{bg}}(x, y, z) = \begin{pmatrix} \overline{u_x}^{x,y}(z) \\ 0 \\ 0 \end{pmatrix},$$

where $\overline{\cdot}^{x,y}$ denotes the classical averaging process with respect to to x and y. As a consequence the background flow in the slender body theory follows:

$$\hat{\mathbf{u}}_{\mathrm{bg}}(s,t) = \mathbf{u}_{\mathrm{bg}}(\boldsymbol{\xi}(s,t)) = \begin{pmatrix} \overline{u_x}^{x,y}(\xi_z(s,t)) \\ 0 \\ 0 \end{pmatrix}.$$

Remark 2.5. From Assumption 2.4, denoting

$$\hat{\mathbb{M}}^{(ij)} = \begin{pmatrix} \hat{m}_{xx}^{(ij)} & \hat{m}_{xy}^{(ij)} & \hat{m}_{xz}^{(ij)} \\ \hat{m}_{yx}^{(ij)} & \hat{m}_{yy}^{(ij)} & \hat{m}_{yz}^{(ij)} \\ \hat{m}_{zx}^{(ij)} & \hat{m}_{zy}^{(ij)} & \hat{m}_{zz}^{(ij)} \end{pmatrix}, \quad \hat{\mathbf{u}}_{\mathrm{cil.}}^{(ij)} = (\hat{u}_{\mathrm{cil.},x}^{(ij)}, \hat{u}_{\mathrm{cil.},y}^{(ij)}, \hat{u}_{\mathrm{cil.},z}^{(ij)}), \quad \hat{\mathbf{u}}_{\mathrm{bg}}^{(ij)} = (\hat{u}_{\mathrm{bg.},x}^{(ij)}, 0, 0),$$

and recalling that $\hat{u}_{\mathrm{cil.},y}^{(ij)} = 0$ and $\hat{m}_{xy}^{(ij)} = \hat{m}_{yx}^{(ij)} = \hat{m}_{yz}^{(ij)} = \hat{m}_{zy}^{(ij)} = 0$ (see Rem. 2.3), we can write:

$$\hat{\mathbf{f}}_{ij}[\mathbf{u}] = \underbrace{\begin{pmatrix} \hat{m}_{xx}^{(ij)} \hat{u}_{\mathrm{cil.},x}^{(ij)} + \hat{m}_{xz}^{(ij)} \hat{u}_{\mathrm{cil.},z}^{(ij)} \\ 0 \\ \hat{m}_{zx}^{(ij)} \hat{u}_{\mathrm{cil.},x}^{(ij)} + \hat{m}_{zz}^{(ij)} \hat{u}_{\mathrm{cil.},z}^{(ij)} \end{pmatrix}}_{\hat{\mathbf{f}}_{ij}^0} - \underbrace{\begin{pmatrix} \hat{m}_{xx}^{(ij)} \\ 0 \\ \hat{m}_{zx}^{(ij)} \end{pmatrix}}_{\hat{\mathbf{m}}^{(ij)}} \hat{u}_{\mathrm{bg},x}^{(ij)}.$$

This allows us to consider the force as the summation of the contribution due to isolated cilia and a contribution due to the background flow, namely,

$$\hat{\mathbf{f}}_{ij}[\mathbf{u}](s,t) = \hat{\mathbf{f}}_{ij}^0(s,t) - \overline{u_x}^{x,y}(\xi_z^{(ij)}(s,t))\, \hat{\mathbf{m}}^{(ij)}(s,t).$$

As a straightforward consequence, the momentum equation in System (2.2) writes:

$$-\mathrm{div}(\mu \nabla \mathbf{u}) + \sum_{i,j} \overline{u}_x^{x,y} \mathbf{m}^{(ij)} \delta_{\Gamma_{ij}} + \nabla p + \gamma \mathbf{e}_z \delta_{\Gamma_*} = \sum_{i,j} \mathbf{f}_{ij}^0 \delta_{\Gamma_{ij}}.$$

It is worthwhile noticing that, due to the background flow:

- the system is linear but...
- the system is *nonlocal*.

Remark 2.6. Note that in the 3D model the punctual value of u_x is not defined on Γ_{ij} because of the loss of regularity induced by the lineic Dirac mass. However the averaging process over the velocity field does not suffer the same drawback: $\overline{u_x}^{x,y}$ is well defined on $(0, L_z)$ and, by extension, on Γ_{ij}.

Variational formulation

Because of the singularity induced by the lineic Dirac source term, the functional framework requires some adaptation with respect to the classical one. Let us temporarily omit time t (which plays the role of a parameter) for the sake of simplicity, we aim at writing the variational formulation of the 3D problem (restoring time t in the notations does not raise any difficulty). The source term $\delta_{\Gamma_{ij}}$ satisfies $\delta_{\Gamma_{ij}} \in (W^{1,r^*}(\Omega))'$ with $r^* > 2$. Let

$$\mathcal{V}_{r^*} := \{\mathbf{v} = (v_x, v_y, v_z) \in (W^{1,r^*}(\Omega))^3,\ \mathbf{v}_{|\Gamma_\downarrow} = 0 \text{ in } (L^{r^*}(\Gamma_\downarrow))^3,\ v_{z|\Gamma_\uparrow} = 0 \text{ in } L^{r^*}(\Gamma_\uparrow),\ v_{z|\Gamma_*} = 0 \text{ in } L^{r^*}(\Gamma_*)\}$$

and $(\mathcal{V}_{r^*})'$ its dual space. The variational formulation requires some precision on the source term. Let $\mathbf{v} \in \mathcal{V}_{r^*}$. We have

$$\begin{aligned}\left\langle \mathbf{f}_{ij}[\mathbf{u}]\delta_{\Gamma_{ij}}, \mathbf{v}\right\rangle_{(\mathcal{V}_{r^*})',\mathcal{V}_{r^*}} &= \int_{\Gamma^{(ij)}(t)} \mathbf{f}_{ij}[\mathbf{u}](x,y,z)\cdot\mathbf{v}(x,y,z)\,\mathrm{d}x\,\mathrm{d}y\,\mathrm{d}z \\ &= \int_0^L \mathbf{f}_{ij}[\mathbf{u}](\boldsymbol{\xi}^{(ij)}(s))\cdot\mathbf{v}(\boldsymbol{\xi}^{(ij)}(s))\,|\nabla\boldsymbol{\xi}^{(ij)}(s)|\,\mathrm{d}s \\ &= \int_0^L \left[\hat{\mathbf{f}}^0_{ij}(s) - \overline{u_x}^{x,y}(\xi_z^{(ij)}(s))\,\hat{\mathbf{m}}^{(ij)}(s)\right]\cdot\mathbf{v}(\boldsymbol{\xi}^{(ij)}(s))\,|\nabla\boldsymbol{\xi}^{(ij)}(s)|\,\mathrm{d}s.\end{aligned}$$

The source term thus contains two contributions:

- a classical contribution due to the action of each isolated cilium:

$$\int_0^L \hat{\mathbf{f}}^0_{ij}(s)\cdot\mathbf{v}(\boldsymbol{\xi}^{(ij)}(s))\,|\nabla\boldsymbol{\xi}^{(ij)}(s)|\,\mathrm{d}s$$

- a nonlocal contribution due to the background flow:

$$\int_0^L \left[\overline{u_x}^{x,y}(\xi_z^{(ij)}(s))\,\hat{\mathbf{m}}^{(ij)}(s)\right]\cdot\mathbf{v}(\boldsymbol{\xi}^{(ij)}(s))\,|\nabla\boldsymbol{\xi}^{(ij)}(s)|\,\mathrm{d}s.$$

Let $r = \frac{r^*}{r^*-1}$, so that $1 \le r < 2$. The variational formulation writes:

$$\left\{\begin{array}{l}\text{find } \mathbf{u}\in\mathcal{V}_r,\ p\in L^r_0(\Omega) \text{ such that} \\ \quad a(\mathbf{u},\mathbf{v}) + nl(\mathbf{u},\mathbf{v}) - b(p,\mathbf{v}) = \ell(\mathbf{v}), \quad \forall \mathbf{v}\in\mathcal{V}_{r^*}, \\ \qquad\qquad\qquad\qquad b(q,\mathbf{u}) = 0, \qquad \forall q\in L^{r^*}_0(\Omega),\end{array}\right. \tag{2.3}$$

with the following bilinear forms

$$\begin{aligned} a(\mathbf{u},\mathbf{v}) &:= \int_\Omega \mu\nabla\mathbf{u}:\nabla\mathbf{v}, \\ nl(\mathbf{u},\mathbf{v}) &:= \textstyle\sum_{i,j}\displaystyle\int_0^L \overline{u_x}^{x,y}(\xi_z^{(ij)}(s))\,\hat{\mathbf{m}}^{(ij)}(s)\cdot\mathbf{v}(\boldsymbol{\xi}^{(ij)}(s))\,|\nabla\boldsymbol{\xi}^{(ij)}(s)|\,\mathrm{d}s, \\ b(p,\mathbf{v}) &:= \int_\Omega p\,\mathrm{div}(\mathbf{v}),\end{aligned}$$

and the following linear form

$$\ell(\mathbf{v}) := \sum_{i,j}\int_0^L \hat{\mathbf{f}}^0_{ij}(s)\cdot\mathbf{v}(\boldsymbol{\xi}^{(ij)}(s))\,|\nabla\boldsymbol{\xi}^{(ij)}(s)|\,\mathrm{d}s.$$

The well-posedness of this problem will be proved in the next section.

3. Derivation of a one-dimensional average model

We propose a way to deal with the averaged velocity term in the 3D model (2.3) and avoid the difficult numerical treatment of the non-local term. It consists in averaging the 3D equations in the x and y directions, taking advantage of the periodic conditions, in order to obtain a 1D equation on $\overline{u_x}^{x,y}$. The numerical solution of this equation can then be injected into the 3D problem. Besides, the existence and uniqueness of the solution to this 1D equation allows to prove the well-posedness of the 3D problem (2.3).

Averaged equations

The averaging process is detailed in Appendix and leads to the following reduced model:

$$\left\{\begin{array}{rl} -\partial_z(\mu\partial_z\overline{u_x}^{x,y}) = \displaystyle\sum_{i,j}\overline{f_{ij,x}[\overline{u_x}^{x,y}]\delta_\Gamma}^{x,y} & \text{in } \mathcal{D}'(0,L_z), \\ \overline{u_x}^{x,y}(0) = 0, & \\ \partial_z\overline{u_x}^{x,y}(L_z) = 0. & \end{array}\right. \tag{3.1}$$

Each source term in the sum over i and j is a distribution in $\mathcal{D}'(0,L_z)$ that needs to be defined properly, since its derivation follows from the averaging process with respect to x and y of the 3D singular source terms, which is not straightforward. Choosing $v := v(z)$, we define

$$\left\langle \overline{f_x\delta}^{x,y}, v\right\rangle_{\mathcal{D}'(0,L_z),\mathcal{D}(0,L_z)} = \frac{1}{L_xL_y}\left\langle f_x\delta, \tilde{v}\right\rangle_{\mathcal{D}'(\Omega),\mathcal{D}(\Omega)}$$

by considering the natural extension from $(0,L_z)$ to Ω (we recall that Ω is periodic in x and y):

$$\begin{array}{rccc} \tilde{\cdot} & : & \mathcal{D}(0,L_z) & \mapsto & \mathcal{D}(\Omega) \\ & & [z\mapsto v(z)] & \to & [(x,y,z)\mapsto \tilde{v}(x,y,z) = v(z)]. \end{array}$$

As a consequence, using the parametrization $s\mapsto \boldsymbol{\xi}(s,t)$ of the cilium, each source term reads:

$$\begin{aligned} \left\langle \overline{f_{ij,x}(\cdot,t)\delta_{\Gamma(t)}}^{x,y}, v\right\rangle_{\mathcal{D}'(0,L_z),\mathcal{D}(0,L_z)} &= \frac{1}{L_xL_y}\int_{\Gamma(t)} f_{ij,x}((x,y,z);t)\, v(z)\,\mathrm{d}x\,\mathrm{d}y\,\mathrm{d}z \\ &= \frac{1}{L_xL_y}\int_0^L f_{ij,x}(\boldsymbol{\xi}^{(ij)}(s,t);t)\, v(\xi_z^{(ij)}(s,t))\,|\nabla\boldsymbol{\xi}^{(ij)}(s,t)|\,\mathrm{d}s. \end{aligned}$$

In the context of mucociliary transport,

$$\hat{\mathbf{f}}_{(ij)}[\mathbf{u}](s,t) = \hat{\mathbb{M}}^{(ij)}(s,t)\cdot\left(\hat{\mathbf{u}}_{\text{cil.}}^{(ij)}(s,t) - \begin{pmatrix} \overline{u_x}^{x,y}(\xi_z^{(ij)}(s,t)) \\ 0 \\ 0 \end{pmatrix}\right).$$

Thus

$$\begin{aligned} \left\langle \overline{f_{ij,x}[\overline{u_x}^{x,y}](\cdot,t)\delta_{\Gamma(t)}}^{x,y}, v\right\rangle_{\mathcal{D}'(0,L_z),\mathcal{D}(0,L_z)} &= \frac{1}{L_xL_y}\int_0^L [\hat{m}_{xx}^{(ij)}\hat{u}_{\text{cil.},x}^{(ij)} + \hat{m}_{xz}^{(ij)}\hat{u}_{\text{cil.},z}^{(ij)}](s,t)\, v(\xi_z^{(ij)}(s,t))\,|\nabla\boldsymbol{\xi}^{(ij)}(s,t)|\,\mathrm{d}s \\ &\quad -\frac{1}{L_xL_y}\int_0^L \hat{m}_{xx}^{(ij)}(s,t)\overline{u_x}^{x,y}(\xi_z^{(ij)}(s,t))\, v(\xi_z^{(ij)}(s,t))\,|\nabla\boldsymbol{\xi}^{(ij)}(s,t)|\,\mathrm{d}s. \end{aligned}$$

Let us now introduce the variational formulation associated to the 1D problem. Defining $V = \{v\in H^1(0,L_z),\ v(0)=0\}$, the variational formulation of the reduced problem (including the summation over all

the cilia) reads:

$$\left\{\begin{array}{l} \text{find } \overline{u_x}^{x,y}(\cdot,t) \in V \text{ such that, for all } v \in V, \\ \displaystyle\int_0^{L_z} \mu(z)\,\partial_z \overline{u_x}^{x,y}(z,t)\cdot\partial_z v(z)\,\mathrm{d}z \\ \qquad + \quad \dfrac{1}{L_xL_y}\displaystyle\sum_{i,j}\int_0^L \hat{m}_{xx}^{(ij)}(s,t)\,\overline{u_x}^{x,y}(\xi_z^{(ij)}(s,t);t)\,v(\xi_z^{(ij)}(s,t))\,|\nabla\boldsymbol{\xi}^{(ij)}(s,t)|\,\mathrm{d}s \\ \qquad = \quad \dfrac{1}{L_xL_y}\displaystyle\sum_{i,j}\int_0^L \left(\hat{m}_{xx}^{(ij)}\hat{u}_{\mathrm{cil.},x}^{(ij)} + \hat{m}_{xz}^{(ij)}\hat{u}_{\mathrm{cil.},z}^{(ij)}\right)(s,t)\,v(\xi_z^{(ij)}(s,t))\,|\nabla\boldsymbol{\xi}^{(ij)}(s,t)|\,\mathrm{d}s. \end{array}\right. \tag{3.2}$$

It is worthwhile noticing that the variational formulation of the 1D reduced problem can be derived from the variational formulation of the 3D problem: up to a constant related to the averaging process, it is then sufficient to use a test function $v \in \mathcal{D}(\Omega)$ which does not depend on x and y, then use the periodicity arguments.

We emphasize that the model is rich and simple: the unknown of the reduced model is $z \mapsto \overline{u_x}^{x,y}(z,t)$ *i.e.* the first component of the mean velocity. This is exactly the observable quantity which allows for the quantification of the mucociliary efficiency. Then the 1D problem divides into three contributions:

- a classical second-order 1D operator, modelling a bifluid description of the medium:

$$\int_0^{L_z} \mu(z)\,\partial_z \overline{u_x}^{x,y}(z,t)\cdot\partial_z v(z)\,\mathrm{d}z,$$

- a source term modelling the action of each cilium over the fluid

$$\frac{1}{L_xL_y}\sum_{ij}\int_0^L \left(\hat{m}_{xx}^{(ij)}\hat{u}_{\mathrm{cil.},x}^{(ij)} + \hat{m}_{xz}^{(ij)}\hat{u}_{\mathrm{cil.},z}^{(ij)}\right)(s,t)\,v(\xi_z^{(ij)}(s,t))\,|\nabla\boldsymbol{\xi}^{(ij)}(s)|\,\mathrm{d}s,$$

- a counter-part contribution due to the collective transport:

$$\frac{1}{L_xL_y}\sum_{i,j}\int_0^L \hat{m}_{xx}^{(ij)}(s,t)\,\overline{u_x}^{x,y}(\xi_z^{(ij)}(s,t))\,v(\xi_z^{(ij)}(s))\,|\nabla\boldsymbol{\xi}^{(ij)}(s,t)|\,\mathrm{d}s.$$

Remark 3.1. We point out the fact that if the averaging process is performed over a domain that fits the metachronal wave in the $x-$direction (recall that cilia only evolve in the $x-z$ plane) then the solution of the reduced problem does not depend on time anymore (by invariance of the setting with respect to time), highlighting the notion of *mucociliary elevator*.

Let us conclude this section with the mathematical properties of the 1D problem:

Theorem 3.2. *The 1D problem* (3.2) *admits a unique solution.*

Proof. Well-posedness of the 1D problem is a consequence of Lax-Milgram theorem, noticing (as in the proof of Thm. 3.3) that

$$\hat{m}_{xx}^{(ij)} = \frac{2\pi\mu}{\ln(L/r)}\left(2 - \frac{|\partial_s\xi_x|^2}{\|\partial_s\boldsymbol{\xi}(s,t)\|^2}\right) \geq \frac{2\pi\mu}{\ln(L/r)} > 0.$$

Thus the bilinear form

$$a_{1\mathrm{D}} : (u,v) \mapsto \int_0^{L_z} \mu(z)\,\partial_z u(z)\cdot\partial_z v(z)\,\mathrm{d}z + \frac{1}{L_x L_y}\sum_{i,j}\int_0^{L} \hat{m}_{xx}^{(ij)}(s,t)\,u(\xi_z^{(ij)}(s,t))\,v(\xi_z^{(ij)}(s))\,|\nabla\boldsymbol{\xi}^{(ij)}(s,t)|\,\mathrm{d}s$$

satisfies

$$a_{1\mathrm{D}}(u,u) \geq \min(\mu_1,\mu_2)\|u\|_V^2$$

as V may be equipped with the norm $v \mapsto \|v\|_V := \|\partial_z v\|_{L^2(0,L_z)}$. □

Strong formulation

The easiest way to implement the reduced 1D model relies on the above variational formulation. However it is possible to rewrite the reduced problem in a strong formulation: this requires to interpret the source term. Let us recall that the description of a cilium $\Gamma(t)$ is performed with a parametrization of the form (subscripts (i,j) have been skipped):

$$s \mapsto \boldsymbol{\xi}(s,t) = (\xi_x(s,t),\xi_y(s,t),\xi_z(s,t)).$$

For a function $f(\cdot,t)$, we have used the identity

$$\int_{\Gamma(t)} f((x,y,z);t)\,v(z)\,\mathrm{d}x\,\mathrm{d}y\,\mathrm{d}z = \int_0^L f(\boldsymbol{\xi}(s,t);t)v(\xi_z(s,t))(z)\,|\nabla\boldsymbol{\xi}(s,t)|\,\mathrm{d}s.$$

Now we propose a parametrization that allows us to recover a classical formulation. Instead of using the "natural" parametrization of the cilium, we may use the third component as the leading parameter and describe $\Gamma(t)$ by

$$z \mapsto \boldsymbol{\Phi}(z,t) = (X(z,t),Y(z,t),z).$$

Now defining $h(t) := \max_s(\xi_z(s,t))$ we have

$$\begin{aligned}\int_{\Gamma(t)} f((x,y,z);t)\,v(z)\,\mathrm{d}x\,\mathrm{d}y\,\mathrm{d}z &= \int_0^{h(t)} f(\boldsymbol{\Phi}(z,t);t)\,v(z)\,|\nabla\boldsymbol{\Phi}(z,t)|\,\mathrm{d}z\\ &= \int_0^{L_z} f(\boldsymbol{\Phi}(z,t);t)\,|\nabla\boldsymbol{\Phi}(z,t)|\,\mathbb{1}_{(0,h(t))}(z)\,v(z)\,\mathrm{d}z\end{aligned}$$

which allows us to rewrite the 1D variational formulation (3.2):

$$\left\{\begin{array}{l}\text{find } \overline{u_x}^{x,y}(\cdot,t)\in V \text{ such that, for all } v\in V,\\ \displaystyle\int_0^{L_z}\mu(z)\,\partial_z\overline{u_x}^{x,y}(z,t)\cdot\partial_z v(z)\,\mathrm{d}z\\ \qquad\displaystyle+\frac{1}{L_xL_y}\int_0^{L_z}\left(\sum_{i,j} m_{xx}^{(ij)}(\boldsymbol{\Phi}^{(ij)}(z,t);t)\cdot|\nabla\boldsymbol{\Phi}^{(ij)}(z,t)|\cdot\mathbb{1}_{(0,h^{(ij)}(t))}(z)\right)\cdot\overline{u_x}^{x,y}(z,t)\cdot v(z)\,\mathrm{d}z\\ \qquad\displaystyle=\frac{1}{L_xL_y}\int_0^{L_z}\left(\sum_{i,j}\left[\hat{m}_{xx}^{(ij)}\hat{u}_{\mathrm{cil.},x}^{(ij)}+\hat{m}_{xz}^{(ij)}\hat{u}_{\mathrm{cil.},z}^{(ij)}\right](\boldsymbol{\Phi}^{(ij)}(z,t);t)\cdot|\nabla\boldsymbol{\Phi}^{(ij)}(z,t)|\cdot\mathbb{1}_{(0,h^{(ij)}(t))}(z)\right)\cdot v(z)\,\mathrm{d}z\end{array}\right.$$

with subsequent notations adapted to each cilium, in particular $h^{(i,j)}(t) = \max_s(\xi_z^{(i,j)}(s,t))$. Thus the strong formulation of this problem reads:

$$\begin{cases} -\partial_z(\mu(z)\partial_z\overline{u_x}^{x,y}(z,\cdot)) + c_1(z,\cdot)\cdot\overline{u_x}^{x,y}(z,\cdot) = c_2(z,\cdot), \quad \forall z\in(0,L_z), \\ \overline{u_x}^{x,y}(0,\cdot) = 0, \\ \partial_z\overline{u_x}^{x,y}(L_z,\cdot) = 0. \end{cases} \tag{3.3}$$

with

$$c_1(z,t) = \frac{1}{L_xL_y}\sum_{i,j} m_{xx}^{(ij)}(\mathbf{\Phi}^{(ij)}(z,t);t)\cdot|\nabla\mathbf{\Phi}^{(ij)}(z,t)|\cdot\mathbb{1}_{(0,h^{(ij)}(t))}(z),$$
$$c_2(z,t) = \frac{1}{L_xL_y}\sum_{i,j}\left[\hat{m}_{xx}^{(ij)}\hat{u}_{\text{cil.},x}^{(ij)} + \hat{m}_{xz}^{(ij)}\hat{u}_{\text{cil.},z}^{(ij)}\right](\mathbf{\Phi}^{(ij)}(z,t);t)\cdot|\nabla\mathbf{\Phi}^{(ij)}(z,t)|\cdot\mathbb{1}_{(0,h^{(ij)}(t))}(z).$$

The use of the strong formulation (3.3) is quite limited in terms of numerical computations as the evaluation of c_1 and c_2 may be intricate. However numerical computations may be easily led with the variational formulation (3.2) whereas the strong formulation (3.3) is helpful for understanding the mathematical structure of the reduced problem. In particular:

- coefficients c_1 and c_2 concentrate all the effects of the active cilia, by a summation process;
- the average velocity $\overline{u_x}^{x,y}$ is continuous with respect to z;
- it is worthwhile noticing that

$$c_1(z,\cdot) = c_2(z,\cdot) = 0 \quad \text{if } z > h := \max_{i,j} h^{(ij)}.$$

  Here h denotes the altitude above which no cilium emerges: in this *passive* area, the average velocity $\overline{u_x}^{x,y}$ is constant (because of the homogeneous Neumann boundary condition).

Well-posedness of the 3D problem

We can now prove the well-posedness of the 3D problem (2.3).

Theorem 3.3. *The 3D problem (2.3) admits a unique solution.*

Proof. Let $\overline{u_x}^{x,y}$ be the unique solution of the 1D problem, and define $\mathcal{W}_{r^*} := \{\mathbf{v} = (v_x, v_y, v_z) \in \mathcal{V}_{r^*},\ \text{div}(\mathbf{v}) = 0\}$. It is straightforward that problem (2.3) is equivalent to

$$\begin{cases} \text{find } \mathbf{u}\in\mathcal{W}_r \text{ such that} \\ a(\mathbf{u},\mathbf{v}) \quad = \quad \tilde{\ell}[\overline{u_x}^{x,y}](\mathbf{v}), \quad \forall\mathbf{v}\in\mathcal{W}_{r^*}, \end{cases} \tag{3.4}$$

where

$$\tilde{\ell}[\overline{u_x}^{x,y}](\mathbf{v}) := \ell(\mathbf{v}) - \textstyle\sum_{i,j}\displaystyle\int_0^L \overline{u_x}^{x,y}(\xi_z^{(ij)}(s))\,\hat{\mathbf{m}}^{(ij)}(s)\cdot\mathbf{v}(\boldsymbol{\xi}^{(ij)}(s))\,|\nabla\boldsymbol{\xi}^{(ij)}(s)|\,\mathrm{d}s,$$

Well-posedness of (3.4) follows from a representation theorem in reflexive Banach spaces (see Thm. 1 in [45]), which we apply to the Sobolev spaces $\mathcal{W}_r$ and $\mathcal{W}_{r^*}$. The bilinear form $a(,.)$ is continuous on $\mathcal{W}_r\times\mathcal{W}_{r^*}$, and non-degenerate with respect to the second variable (this follows from the coercivity of $a(\cdot,\cdot)$ on $H_0^1\times H_0^1$). Then,

a necessary and sufficient condition for (3.4) to admit a unique solution is that there exists a positive number $\alpha > 0$ such that for each $\mathbf{u} \in \mathcal{W}_r$:

$$\sup_{\|\mathbf{v}\|_{\mathcal{W}_{r^*}}=1} a(\mathbf{u}, \mathbf{v}) \geq \alpha \|\mathbf{u}\|_{\mathcal{W}_r}.$$

This property is proven in [46] for a general class of elliptic bilinear operators which are strongly uniformly elliptic and include the case of the bilinear form $a(\cdot, \cdot)$. □

4. Application to mucociliary transport in the lung

The 3D and 1D models presented in the previous sections to simulate many thin structures in a viscous fluid may be investigated through the simulation of mucociliary transport.

4.1. Numerical methods

Unless otherwise stated, the parameters are the ones used in all the simulations. Data related to the fluid domain $\Omega = (0, L_x) \times (0, L_y) \times (0, L_z)$ are the following ones:

$$L_x = 30\,\mu\text{m}, \quad L_y = 4.8\,\mu\text{m}, \quad L_z = 10\,\mu\text{m}.$$

The airway surface liquid is composed of two overlayed layers: the periciliary layer (located in the region $\{(x, y, z) \in \Omega,\ 0 < z < H\}$) and the mucus (located in the region $\{(x, y, z) \in \Omega,\ H < z < L_z\}$). Viscosity of the periciliary layer is $\mu_1 = 1 \times 10^{+0}\,\text{mPa} \cdot \text{s}$ and viscosity of the mucus is $\mu_2 = 1 \times 10^{+4}\,\text{mPa} \cdot \text{s}$. Moreover the interface between the two layers is defined as $\{(x, y, z) \in \Omega,\ z = H\}$ with $H = 4.8\,\mu\text{m}$.

Table 2 summarizes the data related to the cilia, as given in [42]. Those default parameter values lead us to consider a forest of 100×16 cilia in the computational domain Ω. The simulations should present the time evolution of the flow field. In our model the movement of the cilia is prescribed, and it is periodic (the period T is $1/f$). We recall that we need to retrieve the distribution of forces exerted by the cilia on the fluid from their prescribed movement, and for that purpose we use relation (2.1). Now in the case of a two-viscosity fluid this relation, based on the slender-body theory described by Cox [31], is no longer valid. However Fulford and Blake [34] established the expression of the distribution of forces along a slender body which straddles an interface. At the first order (in the regime $\ln(L/r)^{-1}$ tends to zero) and far from the interface, the expression of the force is the same as for constant viscosity. Close to the interface, more precisely at a distance smaller than the radius a of the body, relation (2.1) is no more valid and should be corrected. In our case, we neglect this correction and we consider expression (2.1) for the forces along the whole cilium with a variable viscosity.

Solving the 1D reduced model

The 1D reduced model is solved using the variational formulation (3.2). More precisely we solve a finite-element approximation of (3.2). Define a regular triangulation of $[0, L_z]$, denoted $\mathcal{T}_{h_z}$, that involves N_z nodes (set $h_z = \frac{L_z}{N_z}$) and

$$V_{h_z} := \{v \in \mathcal{C}^0([0, L_z]), v_{|T} \in P_1[T], \forall T \in \mathcal{T}_{h_z} \text{ and } v(0) = 0\}.$$

In the numerical approximation of problem (3.2), we substitute functional space V by the subspace V_{h_z}.

Solving the 3D model

The 3D model is solved using the variational formulation (3.4) once the averaged solution $(\overline{u_x}^{x,y})_h$ has been determined and the resolution is based on a finite-element approximation of the problem. Define a regular triangulation of Ω, denoted $\mathcal{T}_h$, that involves $N_x \times N_y \times N_z$ nodes and the following approximation spaces:

TABLE 2. Summary of data for fluid cilia in the lung, from [42].

Fluid			
Domain dimensions:			
– in axial direction	L_x	30.0	µm
– in azimuthal direction	L_y	4.8	µm
– in radial direction	L_z	10.0	µm
Fluid viscosity in PCL	μ_1	$1 \times 10^{+0}$	mPa · s
Fluid viscosity in mucus	μ_2	$1 \times 10^{+4}$	mPa · s
Airway surface liquid (ASL)	H	4.8	µm
Cilia			
Length of a cilium	L	6.0	µm
Cross-sectional radius of a cilium	a	0.1	µm
Beat frequency of a cilium	f	15.0	Hz
In axial direction:			
– Number of cilia in the computational domain	n_x	100	
– Cilia spacing	ℓ_x^0	0.3	µm
– Number of cilia per unit length	d_x	3.33	μm^{-1}
In azimuthal direction:			
– Number of cilia in the computational domain	n_y	16	
– Cilia spacing	ℓ_y^0	0.3	µm
– Number of cilia per unit length	d_y	3.33	μm^{-1}
Density of cilia	$D_{\text{cil.}}$	11.11	μm^{-2}
Metachronal wavelength	λ	30.0	µm

- for the velocity field:

$$\mathcal{V}_h := \{\mathbf{v} \in (\mathcal{C}^0(\overline{\Omega}))^3,\ \mathbf{v}_{|T} \in (P_1[T] \oplus \text{span}(b_T))^3,\ \forall T \in \mathcal{T}_h \text{ and } \mathbf{v}_{|\Gamma_\downarrow} = 0,\ v_{z|\Gamma_\uparrow} = 0 \text{ and } v_{z|\Gamma_*} = 0\},$$

  where the so-called bubble-function b_T is defined by

$$b_T(\mathbf{x}) = \begin{cases} \lambda_1^T(\mathbf{x}) \cdot \lambda_2^T(\mathbf{x}) \cdot \lambda_3^T(\mathbf{x}), & \text{if } \mathbf{x} \in T, \\ 0, & \text{otherwise,} \end{cases}$$

  and λ_1^T, λ_2^T, λ_3^T are the barycentric coordinates of $\mathbf{x}$ in relation to the mesh element T.
- for the pressure field:

$$\mathcal{W}_h := \{q \in \mathcal{C}^0(\overline{\Omega}),\ q_{|T} \in P_1[T],\ \forall T \in \mathcal{T}_h\}.$$

In the discrete setting, we now consider the variational problem:

$$\begin{cases} \text{find } \mathbf{u}_h \in \mathcal{V}_h,\ p_h \in \mathcal{W}_h \text{ such that} \\ a(\mathbf{u}_h, \mathbf{v}_h) - b(p_h, \mathbf{v}_h) + \varepsilon d(p_h, q_h) = \tilde{\ell}[(\overline{u_x}^{x,y})_h](\mathbf{v}_h), \quad \forall \mathbf{v}_h \in \mathcal{V}_h, \\ b(q_h, \mathbf{u}_h) = 0, \quad \forall q_h \in \mathcal{W}_h. \end{cases} \tag{4.1}$$

Notice that a small perturbative term $d(p_h, q_h) := \int_\Omega p_h q_h$ with factor $\varepsilon \ll 1$ has been introduced in order to fix the constant associated to the pressure field which is determined up to a constant in the initial problem.

Remark 4.1. The main difficulty of the 3D problem relies on its nonlocal property, due to the background flow. It means that the direct resolution of the problem is associated to a linear system involving matrix which

is not sparse. In our case, we took advantage of the 1D reduced model to overcome this difficulty, reducing the complexity to the one of a classical Stokes problem (up to the resolution of a 1D problem that provides the mean velocity that is used as a source term in the subsequent 3D problem). An alternative way to solve the 3D problem consists in using the linearity of the problem to avoid the resolution of the linear system with a full matrix: for this, let us recall that the finite element approximation of the background flow velocity $\overline{u_x}^{x,y}$ is decomposed on a P_1 finite element basis $\{\phi_k\}_{k=1,\dots,N_z}$ with $\phi_k(z_i) = \delta_{ik}$, $\{z_k\}_{k=1,\dots,N_z}$ being the nodes of the 1D mesh. Then define the following problem

$$\left\{\begin{array}{l} \text{find } \mathbf{u}_h^{[0]} \in \mathcal{V}_h,\, p_h^{[0]} \in \mathcal{W}_h,\, \gamma_h^{[0]} \in \mathcal{M}_h \text{ such that} \\ \quad a\left(\mathbf{u}_h^{[0]}, \mathbf{v}_h\right) - b\left(p_h^{[0]}, \mathbf{v}_h\right) + c\left(\gamma_h^{[0]}, \mathbf{v}_h\right) + \varepsilon d\left(p_h^{[0]}, q_h\right) = \ell\left(\mathbf{v}_h\right), \quad \forall \mathbf{v}_h \in \mathcal{V}_h, \\ \qquad\qquad\qquad\qquad\qquad\qquad\qquad\qquad b\left(q_h, \mathbf{u}_h^{[0]}\right) = 0, \qquad \forall q_h \in \mathcal{W}_h, \\ \qquad\qquad\qquad\qquad\qquad\qquad\qquad\qquad c\left(\beta_h, \mathbf{u}_h^{[0]}\right) = 0, \qquad \forall \beta_h \in \mathcal{M}_h, \end{array}\right. \tag{4.2}$$

and also the following N_z auxiliary problems:

$$\left\{\begin{array}{l} \text{find } \mathbf{u}_h^{[k]} \in \mathcal{V}_h,\, p_h^{[k]} \in \mathcal{W}_h,\, \gamma_h^{[k]} \in \mathcal{M}_h \text{ such that} \\ \quad a\left(\mathbf{u}_h^{[k]}, \mathbf{v}_h\right) - b\left(p_h^{[k]}, \mathbf{v}_h\right) + c\left(\gamma_h^{[k]}, \mathbf{v}_h\right) + \varepsilon d\left(p_h^{[k]}, q_h\right) = \ell^{[k]}\left(\mathbf{v}_h\right), \quad \forall \mathbf{v}_h \in \mathcal{V}_h, \\ \qquad\qquad\qquad\qquad\qquad\qquad\qquad\qquad b\left(q_h, \mathbf{u}_h^{[k]}\right) = 0, \qquad \forall q_h \in \mathcal{W}_h, \\ \qquad\qquad\qquad\qquad\qquad\qquad\qquad\qquad c\left(\beta_h, \mathbf{u}_h^{[k]}\right) = 0, \qquad \forall \beta_h \in \mathcal{M}_h, \end{array}\right. \tag{4.3}$$

with

$$\ell^{[k]}(\mathbf{v}_h) = -\sum_{i,j} \int_0^L \phi_k(\xi_z^{(ij)}(s))\, \hat{\mathbf{m}}^{(ij)}(s) \cdot \mathbf{v}(\boldsymbol{\xi}^{(ij)}(s))\, |\nabla \boldsymbol{\xi}^{(ij)}(s)|\, \mathrm{d}s.$$

By linearity, the solution $(\mathbf{u}_h, p_h, \gamma_h)$ is a linear combination of the auxiliary solutions $\{(\mathbf{u}_h^{[k]}, p_h^{[k]}, \gamma_h^{[k]})\}_{k=0,\dots,N_z}$, namely

$$\begin{aligned} \mathbf{u}_h &= \mathbf{u}_h^{[0]} + \sum_{k=1}^{N_z} \lambda_k \mathbf{u}_h^{[k]}, \\ p_h &= p_h^{[0]} + \sum_{k=1}^{N_z} \lambda_k p_h^{[k]}, \\ \gamma_h &= \gamma_h^{[0]} + \sum_{k=1}^{N_z} \lambda_k \gamma_h^{[k]}. \end{aligned} \tag{4.4}$$

It remains to determine $\{\lambda_k\}_k$. Using equation (4.4) in problem (4.1) shows that the linear combination solves the initial problem if

$$\ell + \sum_{k=1}^{N_z} \lambda_k \ell^{[k]} = \widetilde{\ell[\overline{(\mathbf{u}_h)_x}^{x,y}]}$$

that is to say

$$\sum_{k=1}^{N_z} \lambda_k \phi_k = \overline{(\mathbf{u}_h)_x}^{x,y} = \overline{(\mathbf{u}_h^{[0]})_x}^{x,y} + \sum_{k=1}^{N_z} \lambda_k \overline{(\mathbf{u}_h^{[k]})_x}^{x,y}.$$

In order to determine $\{\lambda_k\}_k$, we proceed to the evaluation of the above expression in each 1D node z_i. Denoting $U_i^{[0]} := \overline{(\mathbf{u}_h^{[0]})_x}^{x,y}(z_i)$ and $U_i^{[k]} := \overline{(\mathbf{u}_h^{[k]})_x}^{x,y}(z_i)$ we get

$$\lambda_i = U_i^{[0]} + \sum_{k=1}^{N_z} \lambda_k U_i^{[k]}, \qquad i = 1, ..., N_z.$$

The resolution of the linear system

$$\left[\mathrm{I}_{N_z \times N_z} - \begin{pmatrix} U_1^{[1]} & U_1^{[2]} & \cdots & U_1^{[N_z]} \\ U_2^{[1]} & U_2^{[2]} & \cdots & U_2^{[N_z]} \\ \vdots & \vdots & \ddots & \vdots \\ U_{N_z}^{[1]} & U_{N_z}^{[2]} & \cdots & U_{N_z}^{[N_z]} \end{pmatrix} \right] \cdot \begin{pmatrix} \lambda_1 \\ \lambda_2 \\ \vdots \\ \lambda_{N_z} \end{pmatrix} = \begin{pmatrix} U_1^{[0]} \\ U_2^{[0]} \\ \vdots \\ U_{N_z}^{[0]} \end{pmatrix}$$

determines the solution of the 3D nonlocal problem. However one should notice that this requires, at a preliminary step, the resolution of $N_z + 1$ Stokes problems in 3D, which is much more costly than the approach based upon the resolution of the 1D reduced problem attached to the 3D problem.

4.2. Numerical results

4.2.1. 3D velocity distribution in the reference situation

We have computed the flow produced by a whole forest of cilia, with data given by Table 2: we consider a three dimensional box, with an axial length equivalent to the length of one metachronal wave, $L_x = 30\,\mu\text{m}$, a radial depth of $L_z = 10\,\mu\text{m}$ (which is the average depth of the mucus layer in the human trachea), and an azimuthal width of $L_y = 4.8\,\mu\text{m}$. A 100×16 array of cilia is attached to the bottom of this box and biperiodic boundary conditions on the solution of the Stokes equations are imposed in the axial and azimuthal directions, in order to represent the configuration of an "infinite" array of cilia. The box is filled with a Newtonian fluid with piecewise constant viscosity μ: $\mu = \mu_1$ in the PCL layer and $\mu = \mu_2$ in the mucus layer. The interface between the two layers is located at $z = H$ which is set to $4.8\,\mu\text{m}$, so that cilia penetrate the mucus layer during the effective stroke, but not during the recovery stroke.

Computations have been performed with `FreeFem++`, see [47]: 3D Stokes problems are solved using $\mathrm{P}_1\mathrm{b}$-P_1 finite elements, in order to satisfy a uniform inf-sup condition at the discrete level. Note that in this context the rigorous error analysis has been led in [40]: the method is proven to be convergent with optimal rates when "far from singularities": thus, in our case, error converges to 0 with order 1 in H^1-norm in the mucus region. Note also that the nonlocal term is treated by computing the solution of the average 1D problem: for this, `FreeFem++` is used as well and the resulting 1D solution serves as a contributing source term for the 3D Stokes problem. The 3D problems have been solved with a mesh size

$$N_x \times N_y \times N_z = 100 \times 10 \times 100.$$

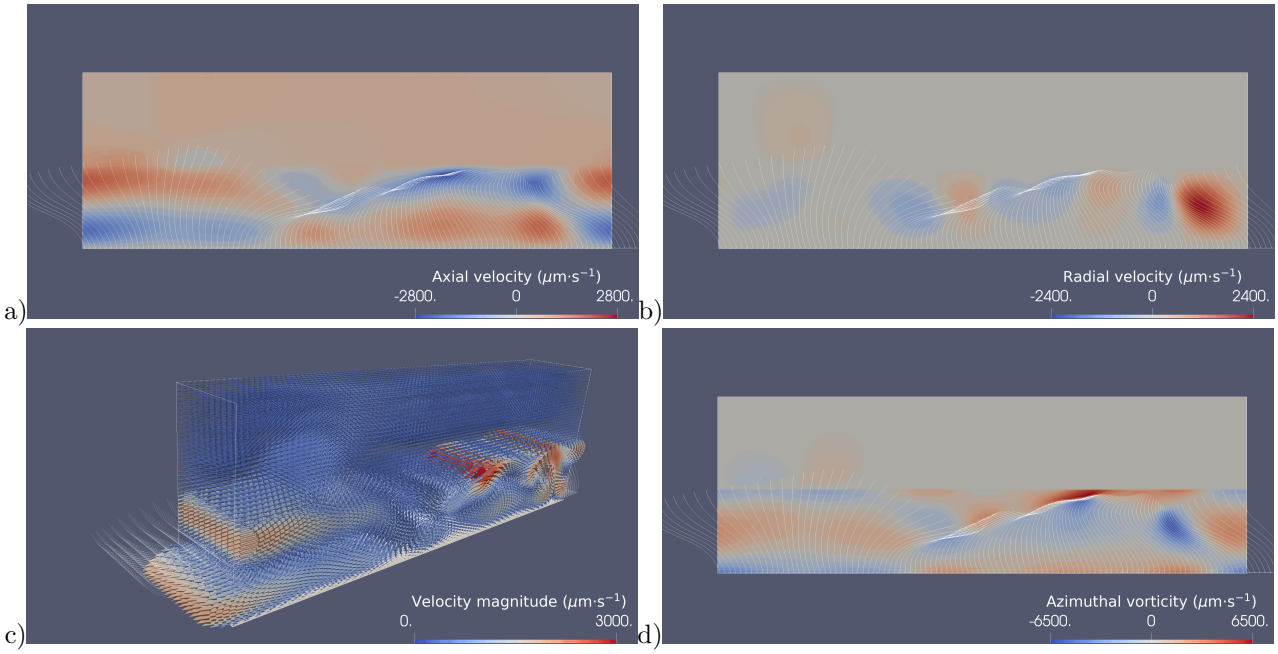

FIGURE 4. Velocity distribution associated to a dense forest of cilia. All data from Table 2.

In particular we choose to limit the number of degrees of freedom in the azimuthal (y) direction as little variation of the velocity field is expected, due to the geometrical configuration; this allows us to use fine mesh in axial (x) and radial (z) directions. Note also that the chosen mesh is conformal with the PCL-mucus interface. The mesh is sufficiently fine to capture the dynamics of the collective ciliary beating with good precision.

Figure 4 illustrates the results obtained in the reference configuration. The density of cilia is high enough for the flow to be independent on time, up to a translation at the velocity of the metachronal wave. As a consequence, drawing one time step only is sufficient. We observe important recirculations in the PCL, with high magnitude variations, while in the mucus layer the flow is rather homogeneous. Actually, mucus is transported at an almost constant velocity, like a block "sliding" over the PCL. To the best of our knowledge, only mucus velocity can be experimentally measured and our numerical results fit the magnitudes of the mucus velocity in experimental measurements: for instance, tracheal mucus velocity is found to be about $100\,\mu\mathrm{m}\cdot\mathrm{s}^{-1}$ in [48, 49], $60\,\mu\mathrm{m}\cdot\mathrm{s}^{-1}$, between 80 and $150\,\mu\mathrm{m}\cdot\mathrm{s}^{-1}$ in [50], $150\,\mu\mathrm{m}\cdot\mathrm{s}^{-1}$ in [51] and it ranges from 160 (young adults) to $110\,\mu\mathrm{m}\cdot\mathrm{s}^{-1}$ (older adults) in [52]. But, as a matter of fact, no experiment gives access to the 3D or axial velocity profile. In a more general way data related to the mucociliary transport are very sparse, often related to morphometric data in small animals (beating frequency, ciliary density...) and the measurement of the mucociliary transport mainly relies on scalar quantities (*e.g.* mean velocity) and not on distributional quantities (such as velocity profiles).

Figures 5 and 6 present the velocity profile for the very same situation as in Figure 4 except that the forest is sparse (50×8 and 25×4 cilia respectively instead of 100×16). We still observe the "block property" of the mucus: this is due to the high viscosity of the mucus, the surface tension at the interface with PCL and the fact that cilia hardly penetrate the mucus. We also observe that in the PCL recirculations are limited when sparsity is enough.

Figure 7 presents the velocity profile for the very same situation as in Figure 4 up to two (major) differences: on the one hand, the viscosity ratio is $\mu_2/\mu_1 = 10^{+0}$ (instead of 10^{+4}) as μ_2 has been set to $\mu_2 = 10^{+0}\,\mathrm{mPa}\cdot\mathrm{s}$; on the other hand, the surface tension constraint has been relaxed (so that the normal velocity at the PCL-mucus interface is not 0). Therefore the situation corresponds to an isoviscous fluid moved by a dense forest of cilia. It

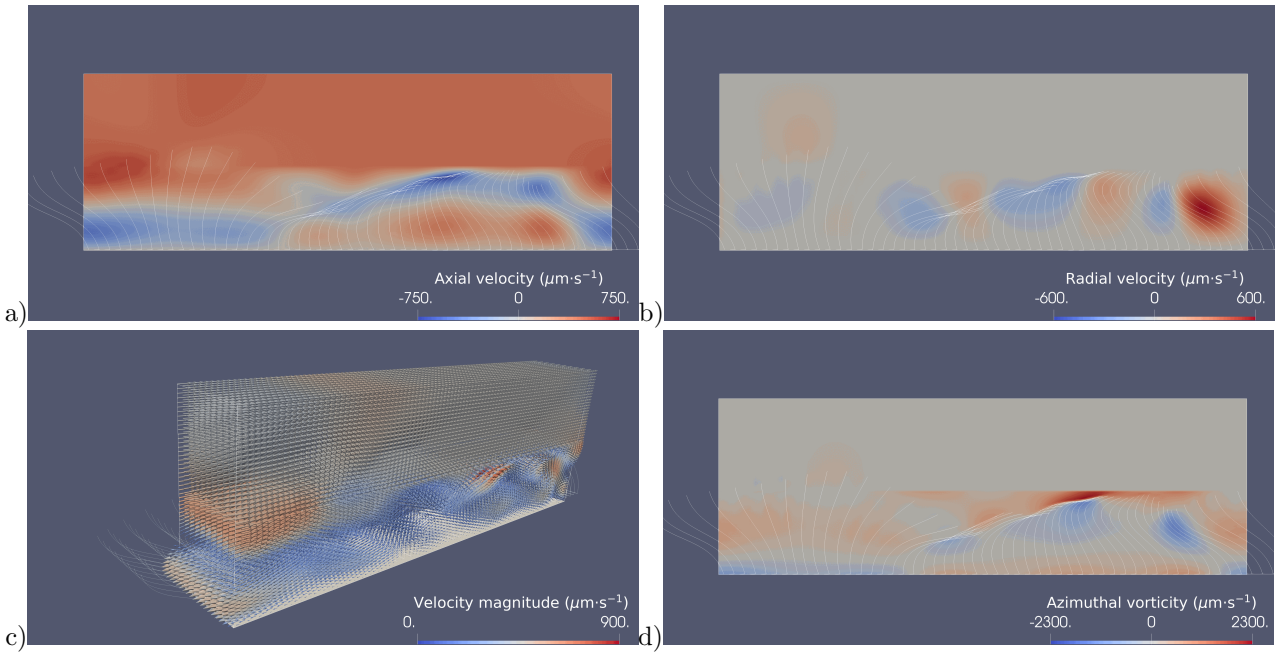

FIGURE 5. Velocity distribution associated to a sparse forest of cilia. Data from Table 2 except for the cilia spacing: $\ell_x^0 = \ell_y^0 = 0.6\,\mu\text{m}$ (instead of $0.3\,\mu\text{m}$) and, as a consequence, the number of cilia has become $n_x = 50$ (instead of 100) and $n_y = 8$ (instead of 16).

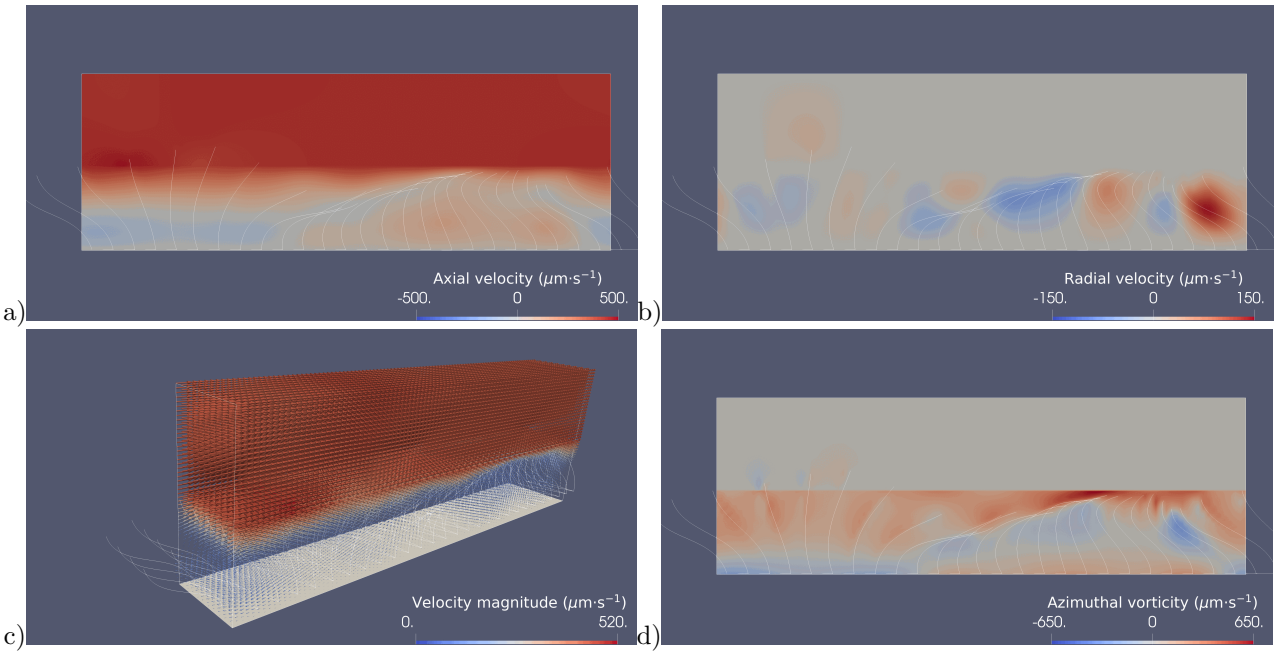

FIGURE 6. Velocity distribution associated to a sparse forest of cilia. Data from Table 2 except for the cilia spacing: $\ell_x^0 = \ell_y^0 = 0.6\,\mu\text{m}$ (instead of $0.3\,\mu\text{m}$) and, as a consequence, the number of cilia has become $n_x = 25$ (instead of 100) and $n_y = 4$ (instead of 16).

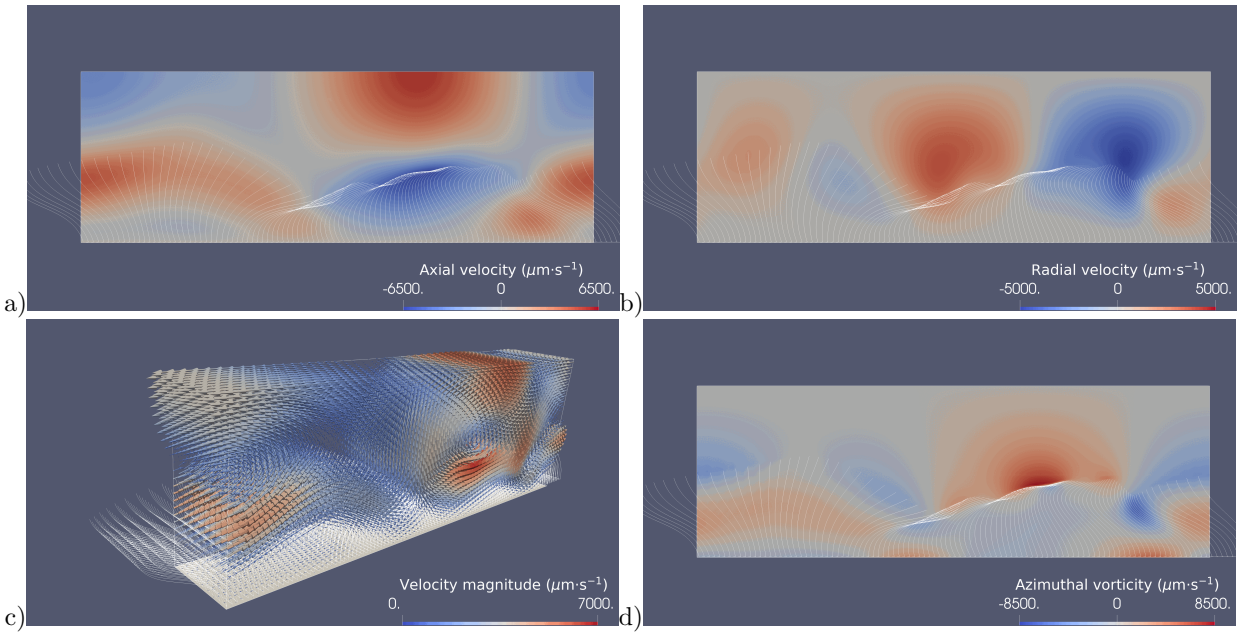

FIGURE 7. Velocity distribution associated to a dense forest of cilia *in the monofluid case* and *relaxing the surface tension constraint*. Data from Table 2 except for the viscosity ratio: $\mu_2 = 1 \times 10^{+0}\,\mathrm{mPa}\cdot\mathrm{s}$.

can be observed that the "block property" of the mucus is not preserved, as velocity variations are significant in the mucus because of the standard viscosity in the whole domain (not only in the PCL) and recirculations are not limited by the surface tension at the interface.

The conclusion is that both high viscosity in the mucus and surface tension allow for a homogeneous flow in the mucus, whereas ciliary density allows for a more efficient mucociliary transport. The impact of these parameters will be investigated in the following subsections.

4.2.2. Influence of the viscosity ratio

Figure 8 presents the influence of the viscosity ratio over the mean axial velocity $z \mapsto u(z) := \overline{u_x}^{x,y}(z)$, resulting from the averaged model (which is also identified as the background flow). This profile is important as it allows for the quantification of the mucociliary efficiency. Data are taken from Table 2, except for the viscosity of the fluid: μ_1 is set to $1 \times 10^{+0}\,\mathrm{mPa}\cdot\mathrm{s}$, whereas μ_2 may vary from $1 \times 10^{+0}$ to $1 \times 10^{+4}\,\mathrm{mPa}\cdot\mathrm{s}$. We observe that the *high viscosity ratio* regime is already nearly achieved for $\mu_2/\mu_1 = 50$, showing some robustness of the mucus transport with respect to μ_2, when sufficiently high.

4.2.3. Influence of the surface tension

Figures 9 and 10 present the numerical results obtained with/without surface tension (all data are taken from Tab. 2). Let us recall that, in equation (2.2), the surface tension γ is the Lagrange multiplier associated to the constraint $\mathbf{u}\cdot\mathbf{n} = 0$ on Γ_* and it ensures the stability of the interface between the PCL and the mucus. The influence of the surface tension is investigated in terms of velocity distribution. As already outlined, it has no influence on the averaged 1D model: the mean axial velocity does not depend on the surface tension. However surface tension has great influence on the 3D velocity distribution, especially when the viscosity ratio is around 1 (monofluid case); the influence of the surface tension tends to be damped for both axial and radial velocities when the viscosity ratio increases.

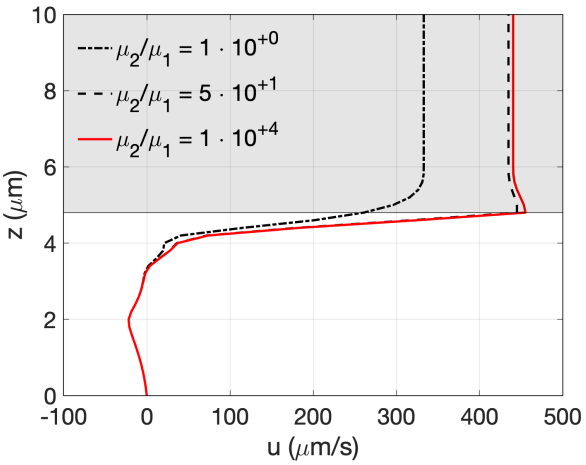

FIGURE 8. Mean axial velocity $z \mapsto u(z) := \overline{u_x}^{x,y}(z)$ in the radial direction, for different viscosity ratios. Data from Table 2, except for mucus viscosity μ_2 (that takes the following values: $1 \times 10^{+0}$, $5 \times 10^{+1}$ and $1 \times 10^{+4}$).

4.2.4. Influence of the position of the ASL

Figure 11 investigates the influence of the position of the PCL-mucus interface on the mucociliary transport, for different viscosity ratios. Actually $H = 4.8\,\mu\text{m}$ is a near-maximizer of the mean mucus velocity. Note that for $H > 6\,\mu\text{m}$, the cilia are completely immersed in the PCL only and do not reach the mucus: as a consequence, the mean axial velocity does not depend on the position of the interface in this regime. But for $H < 6\,\mu\text{m}$, cilia are partially immersed in the mucus, providing energy to the highly viscous fluid in a more direct way. Note that this behaviour quantitatively depends on the viscosity contrast.

Figure 12 investigates the influence of the position of the PCL-mucus interface on the mucociliary transport. Figure 12 a) only depends on the parametrization of the cilia movement (see Tab. 1). The mucus velocity profile exhibits three zones. Range (III) corresponds to $H > 5.9038\,\mu\text{m}$ for which the cilia are completely immersed in the PCL in both effective and recovery strokes: the velocity is constant with respect to H. Range (III) is characterized by the fact that the cilia partially penetrate the mucus in the effective stroke but do not in the recovery stroke: this corresponds to some optimal situation in terms of mucociliary efficiency. In Section (I), cilia penetrate the mucus in the effective stroke but also in the recovery stroke, which explains the decrease of the mucus velocity when compared to the one obtained in Range (II). Note that the mean velocity profile exhibits some discontinuity at the transition between (II) and (III), for high viscosity ratios (actually this trend emerges when the viscosity ratio increases (between 10 and 100) and is stabilized for high viscosity ratios). This is due to some model artefact: in Range (III) the cilia are all immersed in the PCL only; but when we get into Range (II), the head of some cilia penetrate the highly viscous mucus: this leads to local forces that become extremely high (recall that in the slender body theory the force is proportional to the viscosity) with no transition. Thus in this model governed by the slender body theory the energy transferred to the fluid by the cilia is not continuous with respect to H, even if the background flow term stabilizes the solution profiles with respect to high viscosity ratios.

4.2.5. Influence of the ciliary density

Figures 13 and 14 investigate the influence of the ciliary density over the mucociliary transport for $H = 4.8\,\mu\text{m}$ and $H = 6.2\,\mu\text{m}$. Note that

- For $H < 6\,\mu\text{m}$, the cilia penetrate the mucus during the effective stroke;
- For $H > 6\,\mu\text{m}$, the cilia are completely immersed in the PCL only and do not penetrate the mucus.

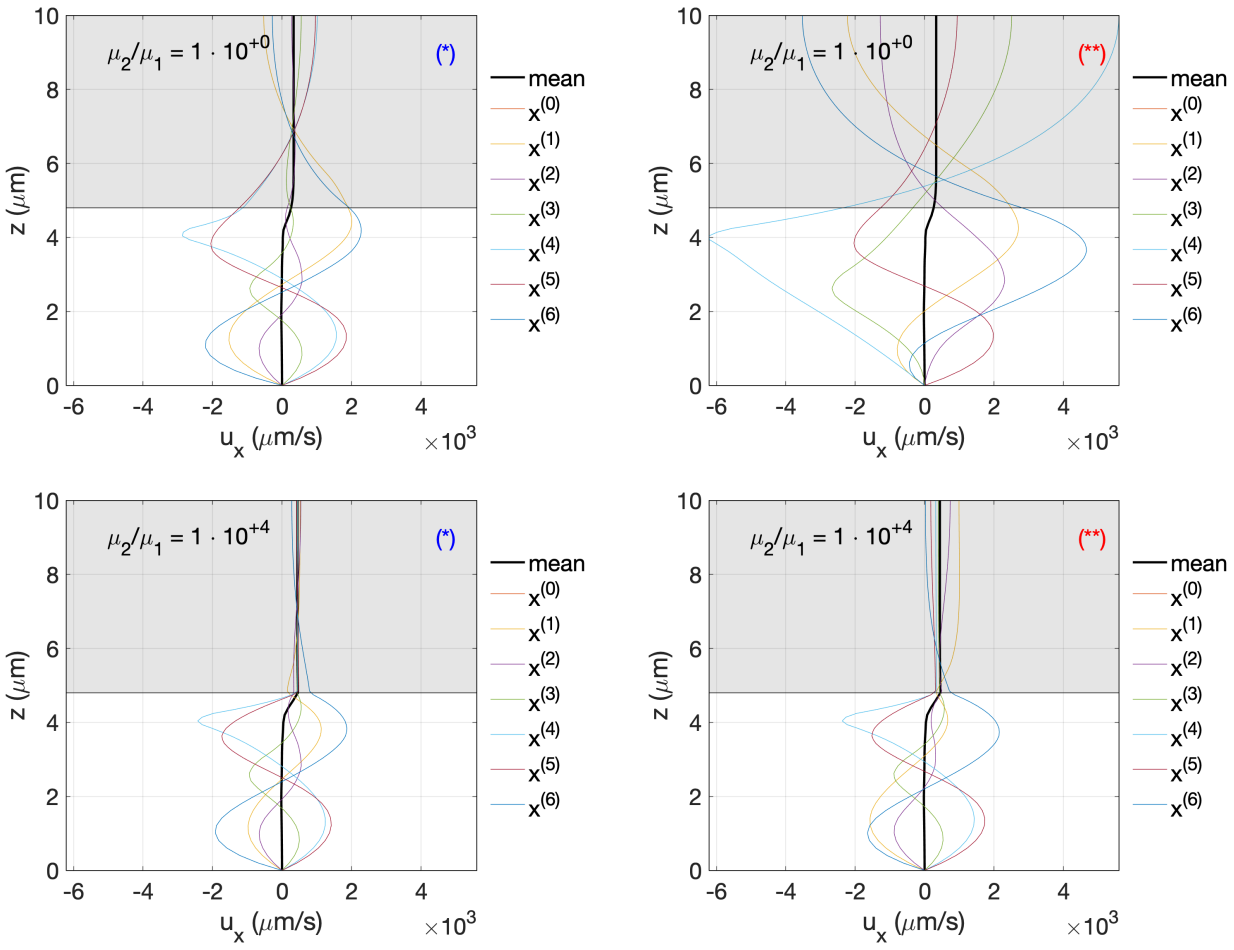

FIGURE 9. Axial velocity profiles in the radial direction, for different axial positions $x = x^{(j)} = j\Delta$ (with $\Delta = 5\,\mu\text{m}$). The velocity is averaged in the azimuthal direction y (note that the velocity little varies in this direction) so that we show the following profiles: $z \mapsto \overline{u_x}^y(x^{(j)}, z)$(∗) refers to the standard model with surface tension (hence $u_z = 0$ is imposed at the PCL-mucus interface) whereas (∗∗) refers to the model in which no surface tension is taken into account (hence u_z is not constrained at the PCL-mucus interface).

Other data are taken from Table 2, except for the cilia densities ℓ_x^0 and ℓ_y^0 (or the number of cilia in each direction, n_x and n_y, as $n_x\ell_x^0 = L_x$ and $n_y\ell_y^0 = L_y$). The reference density of cilia is 11.11 μm^{-2}, which corresponds to a forest of $n_x \times n_y$ cilia with $n_x = 100$ and $n_y = 16$, placed on surface whose area is $L_x \times L_y$ with $L_x = 30.0\,\mu\text{m}$ and $L_y = 4.8\,\mu\text{m}$.

Figure 13 investigates the influence of the ciliary density over the mucociliary transport with $H = 4.8\,\mu\text{m}$. In Figure 13 a), we let d_x vary (whereas the density of cilia in the azimuthal direction is fixed to its reference value). In Figure 13 b), we let d_y vary (whereas the density of cilia in the axial direction is fixed to its reference value). In Figure 13 c), we investigate the crossed influence of the axial/azimuthal densities. We observe that the mucus velocity becomes stable when n_x or n_y increase: these results are due to the background flow term in the 3D model or, equivalently, the counter-part contribution due to the collective transport in the 1D model. Indeed the source term (without background flow) is proportional to n_x and n_y but so does the damping term coefficient due to the background flow. The latter argument prevents the model from being linear with respect to

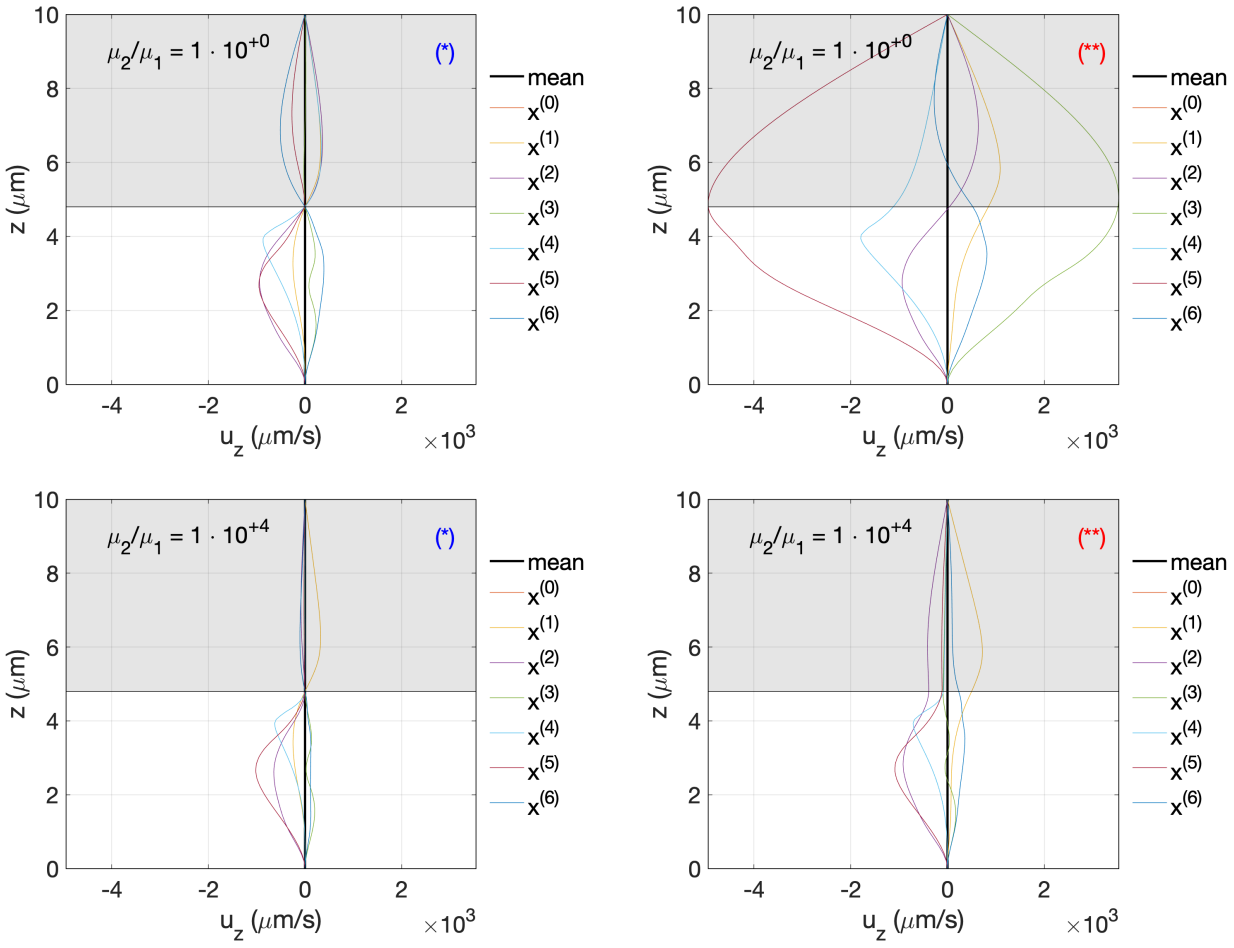

FIGURE 10. Radial velocity profiles in the radial direction, for different axial positions $x = x^{(j)} = j\Delta$ (with $\Delta = 5\,\mu\text{m}$). The velocity is averaged in the azimuthal direction y so that we show the following profiles: $z \mapsto \overline{u_z}^y(x^{(j)}, z)(*)$ refers to the standard model with surface tension (hence $u_z = 0$ is imposed at the PCL-mucus interface) whereas $(**)$ refers to the model in which no surface tension is taken into account (hence u_z is not constrained at the PCL-mucus interface).

n_x and n_y and it provides some remarkable robustness of the mucus transport with respect to the cilia density, when reaching a sufficiently high value.

Figure 14 investigates the influence of the ciliary density over the mucociliary transport with $H = 6.2\,\mu\text{m}$ (instead of $H = 4.8\,\mu\text{m}$). In this case, the cilia do not penetrate the mucus. The mean axial velocity profile does not depend on the position of the interface: this results from the fact that, as long as the cilia do not penetrate the mucus, the mucus area is passive (*i.e.* source term is null) which, combined with homogeneous Neumann condition, leads to a constant velocity profile in the mucus. Noteworthily the robustness of the ciliary transport with respect to the cilia density is achieved when it reaches a sufficiently high value.

Figures 15 and 16 exhibit the axial velocity profiles with low density for $H = 4.8\,\mu\text{m}$ and $H = 6.2\,\mu\text{m}$ respectively. When the cilia penetrate the mucus during the effective stroke (see Fig. 15, corresponding to $H = 4.8\,\mu\text{m}$), we notice that *low* ciliary density does not modify the magnitude of the mean axial velocity, but it damps the dispersion of velocity profiles around the mean profile: the loss of activity makes the velocity

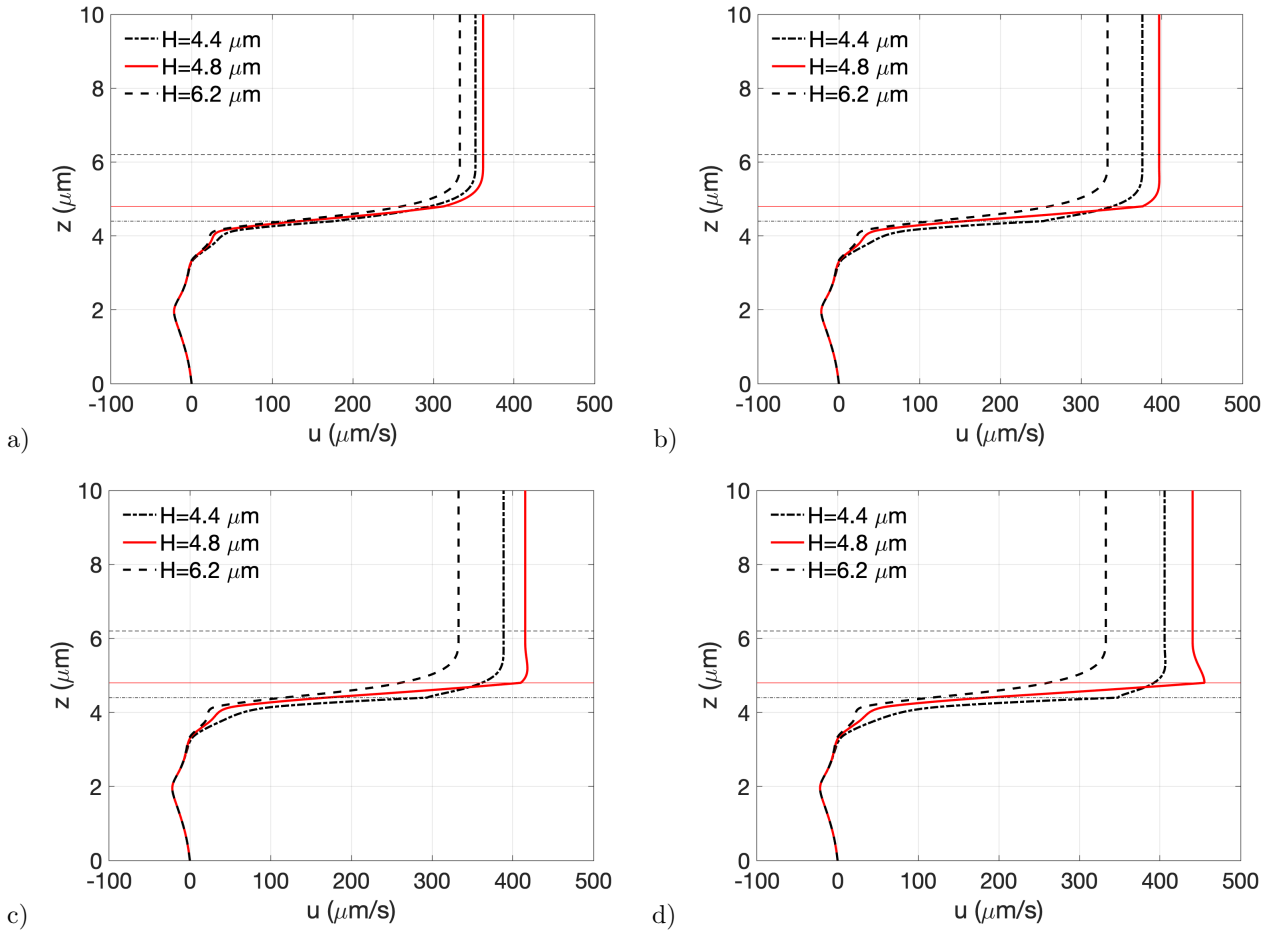

FIGURE 11. Influence of the position of the ASL (H) on the mean axial velocity $z \mapsto \overline{u_x}^{x,y}(z)$ in the radial direction (through PCL and mucus). a) $\mu_2 = 2 \times 10^{+0}\,\mathrm{mPa}\cdot\mathrm{s}$, b) $\mu_2 = 5 \times 10^{+0}\,\mathrm{mPa}\cdot\mathrm{s}$, c) $\mu_2 = 1 \times 10^{+1}\,\mathrm{mPa}\cdot\mathrm{s}$, d) $\mu_2 = 1 \times 10^{+4}\,\mathrm{mPa}\cdot\mathrm{s}$.

distribution more homogeneous, in particular in the PCL. When the cilia do not penetrate the mucus (see Fig. 16, corresponding to $H = 6.2\,\mu\mathrm{m}$), not only dispersion of velocity profiles around the mean profile tends to be damped, but also the magnitude of the mean velocity decreases.

5. Conclusion

In this article we modelled the mucociliary transport through a 3D model connecting all the main features of the process: 1) (dense) forests of cilia immersed in a fluid, with an individual description of the cilia; 2) the fluid is a two-layer fluid (PCL+mucus with a sharp viscosity ratio) separated by an interface which is made stable due to surface tension. The main limitation lies in the fact that the ciliary movement is prescribed and the forces exerted by the cilia on the fluid are evaluated using an approximated formula provided by the slender body theory. Beyond these limitations, the model is based upon fundamental equations of dynamics and results in a nonlocal Stokes system with singular source terms; from the mathematical point of view, the model is well-posed (in suitable functional spaces) and, from the numerical point of view, the computation of the 3D velocity profiles is performed using numerical methods characterized by rigorous error analysis (even in the singular case). Numerical results allow us to describe the 3D velocity distribution in a non-pathological

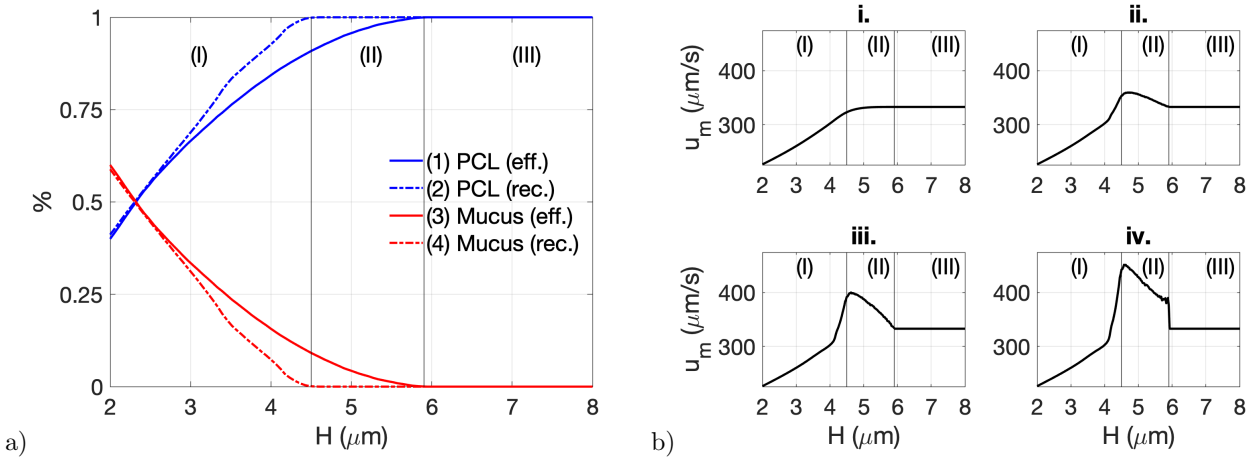

FIGURE 12. Influence of the position of the ASL (H). a) The percentage (%) of time spent by cilia in the mucus and PCL is shown for both phases: effective stroke (eff.) and recovery stroke (rec.). b) Influence of the position of the ASL on mucus velocity $u_m = (L_z - H)^{-1} \int_H^{L_z} \overline{u_x}^{x,y}(z)\,\mathrm{d}z$ for different viscosity ratios (data from Tab. 2, except for the position of the PCL-mucus interface which varies from 2 to 8 µm and the viscosity μ_2 that takes the following values: **i.** $\mu_2 = 1 \times 10^{+0}$ mPa · s, **ii.** $\mu_2 = 2 \times 10^{+0}$ mPa · s, **iii.** $\mu_2 = 5 \times 10^{+0}$ mPa · s, **iv.** $\mu_2 = 1 \times 10^{+4}$ mPa · s).

situation and to highlight, by comparison, the influence of critical parameters (beating frequency of the cilia, mucus viscosity, surface tension, ciliary density in the forest, position of the PCL/mucus interface *etc.*) on the velocity distribution and, finally, on the efficiency of the mucociliary transport. Note that several extensions can be made:

- *Influence of the airflow on the mucociliary efficiency.* In a bronchus, the bronchial wall is lined with a bifluid made of two layers (the PCL and mucus) and the center of the bronchus is filled with air. Thus mucus has an interface not only with PCL (at $\{z = H\}$) but also with air (at $\{z = L_z\}$). In this article, the influence of air has been neglected (hence we impose a free-slip boundary condition at $\{z = L_z\}$) but the influence of air cycles combined with the ciliary activity can be done as follows: because the airflow goes through the bronchus, the shear effect at the air-mucus interface imposed by the respiratory cycle can alternatively increase (at expiration) or decrease (at expiration) the mucus velocity; this phenomenon can be taken into account by introducing a pressure drop in the fluid flow and replacing the free-slip boundary conditions at $\{z = L_z\}$ by boundary conditions that model the shear effect of the air flow in the bronchus, which can be represented by a Poiseuille flow.
- *Viscoelasticity of the mucus.* Viscoelastic properties of the mucus may have an impact on the mucociliary transport, in particular in pathological situations [17, 25]. We could extend our 3D model to take into account viscoelasticity: for instance, using an Oldroyd-type model, under the assumption that cilia do not penetrate the mucus, the constitutive equations relating the elastic tensor to the velocity field can be computed using a splitting scheme combined with a characteristics method as in [53]. If cilia penetrate the mucus, the lack of regularity of the velocity field, due to the singular source term in the active part of the mucus, would certainly lead to mathematical and numerical difficulties: indeed, to the best of our knowledge, the regularity of the solution for the Stokes-Oldroyd problem with singular source term is an open question and, thus, it requires a suitable functional framework in order to derive a rigorous mathematical formulation and error analysis for the finite element method in this case.

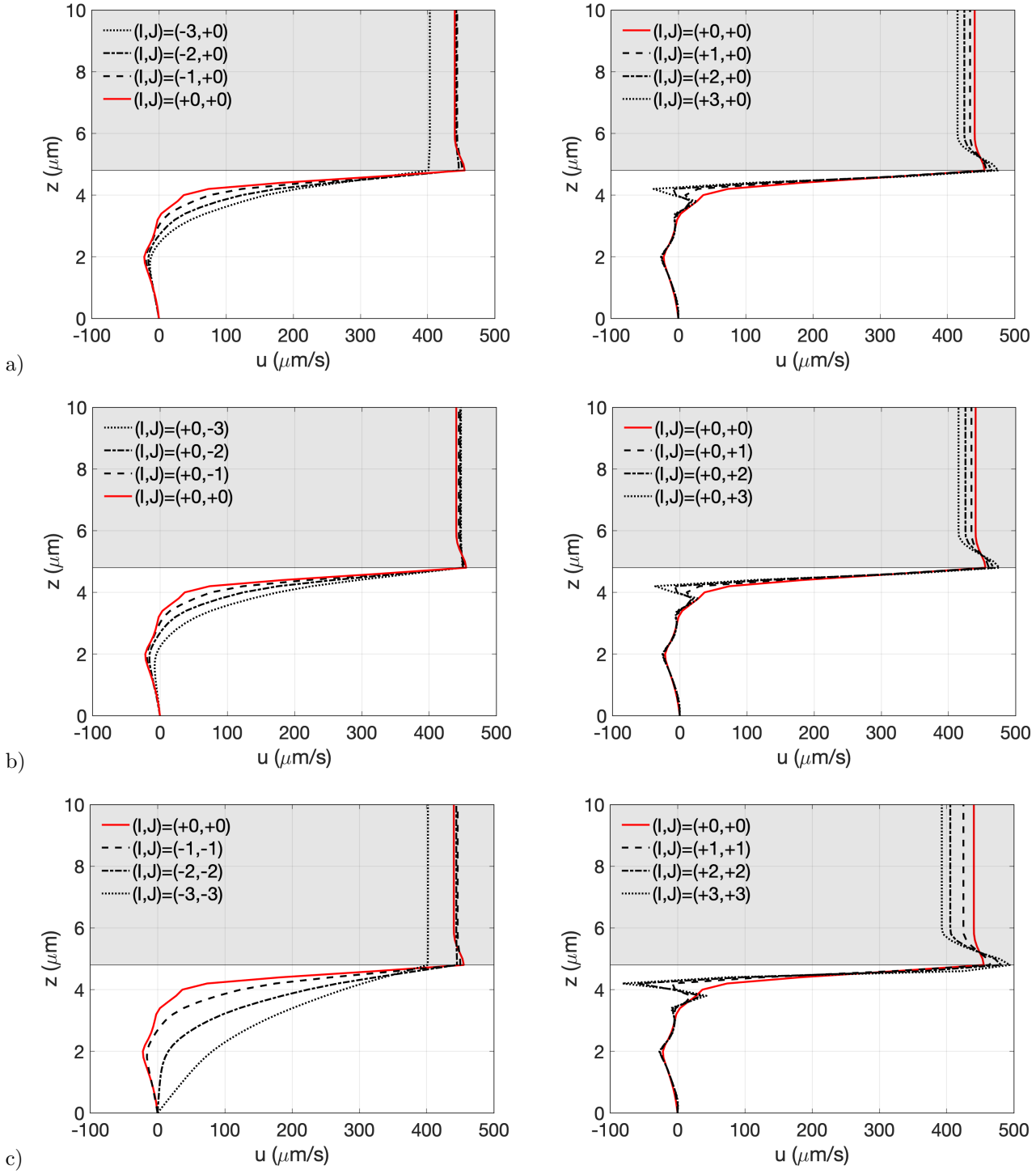

FIGURE 13. Influence of the density of cilia on the mean axial velocity $z \mapsto u(z) := \overline{u_x}^{x,y}(z)$, for $H = 4.8\,\mu\text{m}$. All data from Table 2 except for the density of cilia. Index (I, J) relates to the following density: $d_x = 2^I d_x^0$ (axial direction), $d_y = 2^J d_y^0$ (azimuthal direction), with reference values: $d_x^0 = d_y^0 := 3.33\,\mu\text{m}^{-1}$.

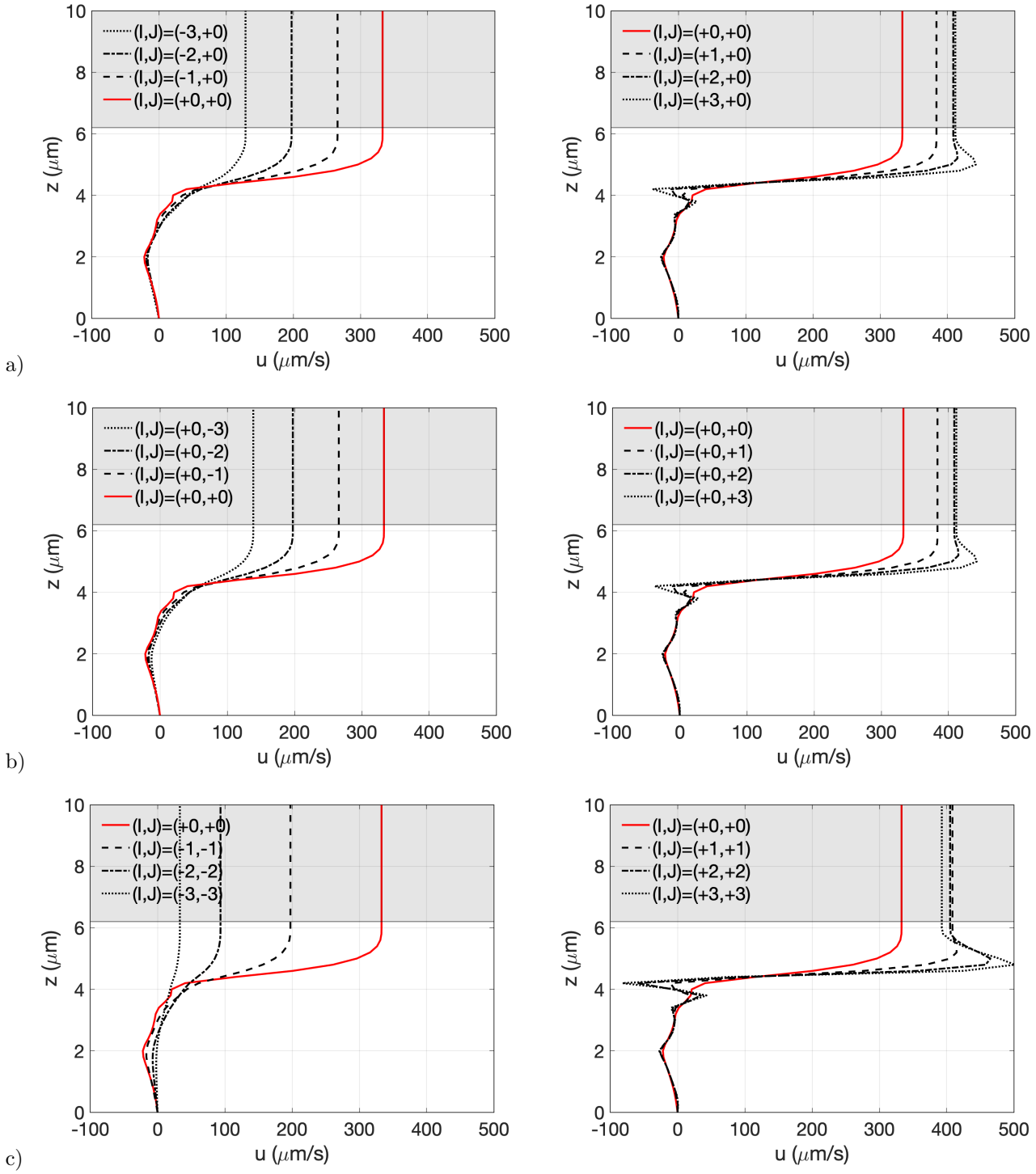

FIGURE 14. Influence of the density of cilia on the mean axial velocity $z \mapsto u(z) := \overline{u_x}^{x,y}(z)$, for $H = 6.2\,\mu\text{m}$. All data from Table 2 except for the density of cilia and the position of the interface. Index (I, J) relates to the following density: $d_x = 2^I d_x^0$ (axial direction), $d_y = 2^J d_y^0$ (azimuthal direction), with reference values: $d_x^0 = d_y^0 := 3.33\,\mu\text{m}^{-1}$.

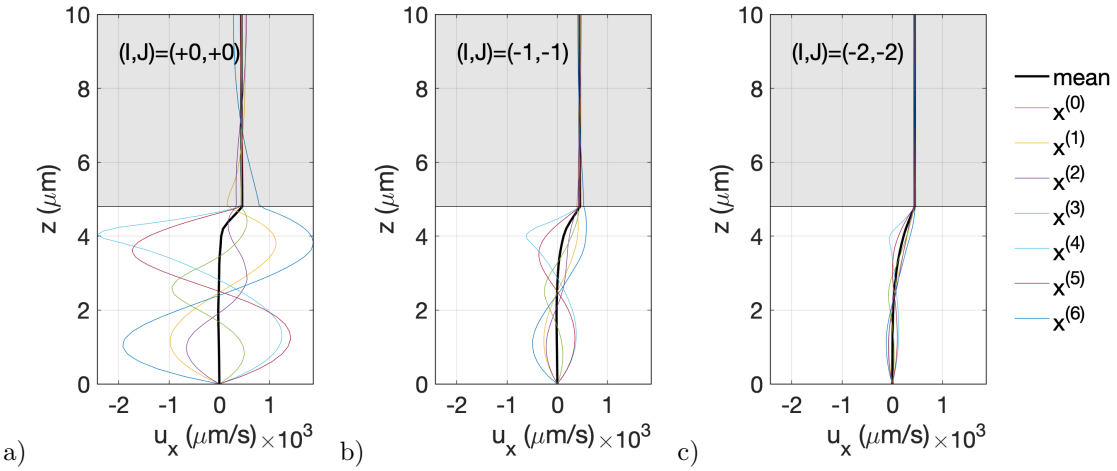

FIGURE 15. Influence of the density of cilia on the axial velocity, for $H = 4.8\,\mu\text{m}$. All data from Table 2 except for the density of cilia. The axial velocity is averaged in the azimuthal direction y (note that the velocity little varies in this direction) so that we show the following profiles: $z \mapsto \overline{u_x}^y(x^{(j)}, z)$ for different axial positions $x = x^{(j)} = j\Delta$ (with $\Delta = 5\,\mu\text{m}$). Index (I, J) relates to the following density: $d_x = 2^I d_x^0$ (axial direction), $d_y = 2^J d_y^0$ (azimuthal direction), with reference values: $d_x^0 = d_y^0 := 3.33\,\mu\text{m}^{-1}$.

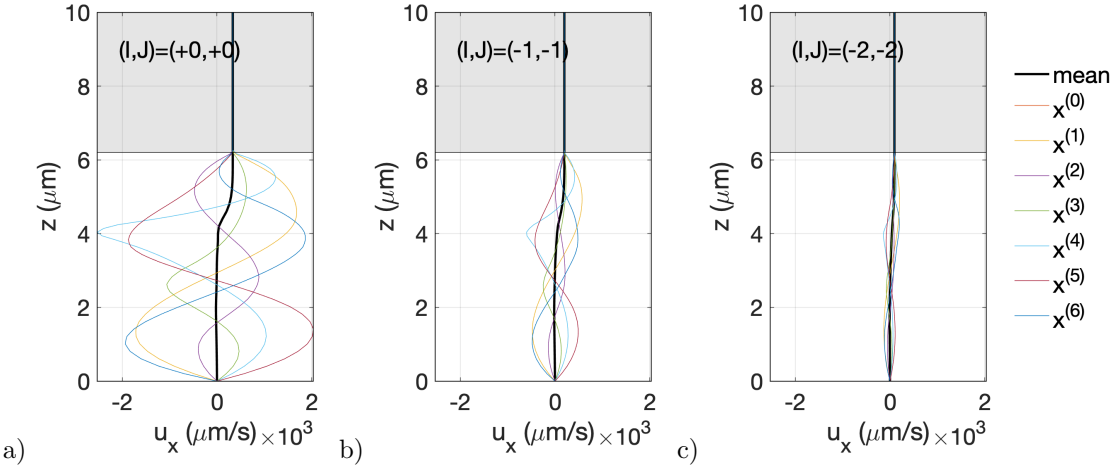

FIGURE 16. Influence of the density of cilia on the axial velocity, for $H = 6.2\,\mu\text{m}$. All data from Table 2 except for the density of cilia. The axial velocity is averaged in the azimuthal direction y (note that the velocity little varies in this direction) so that we show the following profiles: $z \mapsto \overline{u_x}^y(x^{(j)}, z)$ for different axial positions $x = x^{(j)} = j\Delta$ (with $\Delta = 5\,\mu\text{m}$). Index (I, J) relates to the following density: $d_x = 2^I d_x^0$ (axial direction), $d_y = 2^J d_y^0$ (azimuthal direction), with reference values: $d_x^0 = d_y^0 := 3.33\,\mu\text{m}^{-1}$.

Appendix A.

Let us describe the derivation of the reduced model.

Averaging process

We denote by $\overline{\cdot}^{x}$ (resp. $\overline{\cdot}^{y}$; $\overline{\cdot}^{x,y}$) the (classical) averaging process with respect to x (resp. y ; x and y). For instance, for a regular function $(x,y,z)\mapsto f(x,y,z)$ we denote $\overline{f}^{x,y}:(0,L_z)\mapsto\mathbb{R}$ the function defined by

$$\overline{f}^{x,y}(z)=\frac{1}{L_xL_y}\int_0^{L_x}\int_0^{L_y}f(x,y,z)\,\mathrm{d}x\,\mathrm{d}y.$$

Averaging the continuity equation $\partial_x u_x+\partial_y u_y+\partial_z u_z=0$ combined with the periodicity of the velocity field $\mathbf{u}$ yields

$$\partial_z\overline{u_z}^{x,y}=0$$

which, combined with the homogeneous Dirichlet condition at $\Gamma_\downarrow$, gives:

$$\overline{u_z}^{x,y}=0.$$

Let us average the momentum equation. Note that the source terms involved by the ciliary beat are not regular but we first derive the average model by skipping this difficulty which will be treated thereafter. Therefore assume that F_x, F_y and F_z are regular source terms (*e.g.* in $L^2(\Omega)$), we have

$$\begin{cases}
-\partial_x(\mu\partial_x u_x)-\partial_y(\mu\partial_y u_x)-\partial_z(\mu\partial_z u_x)+\partial_x p & = F_x \quad \text{on } \Omega,\\
-\partial_x(\mu\partial_x u_y)-\partial_y(\mu\partial_y u_y)-\partial_z(\mu\partial_z u_y)+\partial_y p & = F_y \quad \text{on } \Omega,\\
-\partial_x(\mu\partial_x u_z)-\partial_y(\mu\partial_y u_z)-\partial_z(\mu\partial_z u_z)+\partial_z p \quad + \quad \gamma\delta_{\Gamma_*} & = F_z \quad \text{on } \Omega.
\end{cases}$$

Averaging in x and y, using the fact that μ only depends on z and using the periodicity of $\mathbf{u}$ and p we obtain

$$\begin{cases}
-\partial_z(\mu\partial_z\overline{u_x}^{x,y}) & = \overline{F_x}^{x,y} \quad \text{on } (0,L_z),\\
-\partial_z(\mu\partial_z\overline{u_y}^{x,y}) & = \overline{F_y}^{x,y} \quad \text{on } (0,L_z),\\
-\partial_z(\mu\partial_z\overline{u_z}^{x,y})+\partial_z\overline{p}^{x,y} \quad + \quad \overline{\gamma}^{x,y}\delta_{z=H} & = \overline{F_z}^{x,y} \quad \text{on } (0,L_z).
\end{cases}$$

Next as the cilia movement only occurs in the $(x-z)$ plane (see the parametrization of the ciliary beat patterns), then $F_y=0$ and the second equation of the system writes:

$$-\partial_z(\mu\partial_z\overline{u_y}^{x,y})=0 \quad \text{on } (0,L_z),$$

which, by the homogeneous boundary condition on $\Gamma_\downarrow$, gives:

$$\overline{u_y}^{x,y}=0.$$

Besides, as previously shown, $\overline{u_z}^{x,y} = 0$ so that the third equation of the system writes

$$\partial_z \overline{p}^{x,y} + \overline{\gamma}^{x,y}\delta_{\Gamma_*} = \overline{F_z}^{x,y} \quad \text{on } (0, L_z).$$

The reduced system (with regular source term) writes

$$\begin{cases} -\partial_z(\mu \partial_z \overline{u_x}^{x,y}) = \overline{F_x}^{x,y} & \text{on } (0, L_z), \\ \overline{u_y}^{x,y} = 0 & \text{on } (0, L_z), \\ \overline{u_z}^{x,y} = 0 & \text{on } (0, L_z), \\ \partial_z \overline{p}^{x,y} + \overline{\gamma}^{x,y}\delta_{z=H} = \overline{F_z}^{x,y} & \text{on } (0, L_z). \end{cases} \tag{A.1}$$

Notice that the last equation relates the average pressure $\overline{p}^{x,y}$ and the surface tension $\overline{\gamma}^{x,y}$ to the force exerted by the cilia onto the fluid. Hower this equation is not required when one aims at determining the average velocity field, in particular $z \mapsto \overline{u_x}^{x,y}(z)$ which describes the average velocity profile of the PCL+mucus system. Additionally let us deal with the boundary conditions. In a straightforward way, the Dirichlet condition readily adapts into:

$$\overline{u_x}^{x,y}(0) = \overline{u_y}^{x,y}(0) = \overline{u_z}^{x,y}(0) = 0.$$

The kinematic and dynamic conditions on $\Gamma_\uparrow$ read $u_z = 0$ and $\partial_z u_x = 0$ on $\Gamma_\uparrow$ which, after averaging in x and y, yields:

$$\begin{cases} \overline{u_z}^{x,y}(L_z) = 0, \\ \partial_z \overline{u_x}^{x,y}(L_z) = 0. \end{cases}$$

As a consequence, the reduced model (with regular source term) reads:

- First component of the velocity:

$$\begin{cases} -\partial_z(\mu(z)\partial_z \overline{u_x}^{x,y}(z)) = \overline{F_x}^{x,y}(z), \quad \forall z \in (0, L_z), \\ \overline{u_x}^{x,y}(0) = 0, \\ \partial_z \overline{u_x}^{x,y}(L_z) = 0. \end{cases} \tag{A.2}$$

- Second component of the velocity:

$$\overline{u_y}^{x,y}(z) = 0, \quad \forall z \in (0, L_z).$$

- Third component of the velocity:

$$\overline{u_z}^{x,y}(z) = 0, \quad \forall z \in (0, L_z).$$

- Pressure field:

$$\partial_z \overline{p}^{x,y}(z) + \overline{\gamma}^{x,y}(z)\delta_{z=H} = \overline{F_z}^{x,y}(z) \quad \forall z \in (0, L_z).$$

Remark A.1. Partial derivatives with respect to z have been maintained because the functions may depend on time, even if it plays the role of a parameter. In particular, if the source terms F_x, F_y and F_z do depend on time, so do the solution $\mathbf{u}$ and its subsequent average first component $\overline{u_x}^{x,y}$.

Reduction of the source term

Let us now provide some details about the derivation of the source terms $\overline{F_x}^{x,y}$ and $\overline{F_z}^{x,y}$ in the context of the ciliary study. More precisely we need to define in a rigorous way the averaging process of the source term defined in Problem (2.2), namely:

$$\mathbf{F} := \begin{pmatrix} F_x \\ F_y \\ F_z \end{pmatrix} = \sum_{i,j} \mathbf{f}_{ij}(\cdot,t)\delta_{\Gamma_{ij}(t)}.$$

In order to define the averaging process for the singular source term, let us deal with one single Dirac term (the extension to an arbitrary number of singular source terms follows from linearity).

For any (i,j), $i \in [\![1, n_x]\!]$ and $j \in [\![1, n_y]\!]$, consider the $(i,j)-$th cilium associated with the source term $\mathbf{f}_{ij}\delta_{\Gamma_{ij}}$ (we omit in this subsection the subscript (i,j), for the sake of simplicity). In the variational formulation of the source term, using a test function $\mathbf{v} \in (\mathcal{D}(\Omega))^3$, the source term would be

$$\left\langle \mathbf{f}(\cdot,t)\delta_{\Gamma(t)}, \mathbf{v} \right\rangle_{(\mathcal{D}'(\Omega))^3,(\mathcal{D}(\Omega))^3} = \int_{\Gamma(t)} \mathbf{f}(\cdot,t)\cdot\mathbf{v}\,\mathrm{d}x\,\mathrm{d}y\,\mathrm{d}z.$$

Aiming at studying the first component of the system, namely choosing $\mathbf{v} = (v,0,0)$, we focus on

$$\left\langle f_x(\cdot,t)\delta_{\Gamma(t)}, v \right\rangle_{\mathcal{D}'(\Omega),\mathcal{D}(\Omega)} = \int_{\Gamma(t)} f_x(\cdot,t)\,v\,\mathrm{d}x\,\mathrm{d}y\,\mathrm{d}z.$$

Next choosing $v := v(z)$, we define

$$\left\langle \overline{f_x(\cdot,t)\delta_{\Gamma(t)}}^{x,y}, v \right\rangle_{\mathcal{D}'(0,L_z),\mathcal{D}(0,L_z)} = \frac{1}{L_xL_y}\left\langle f_x(\cdot,t)\delta_{\Gamma(t)}, \tilde{v} \right\rangle_{\mathcal{D}'(\Omega),\mathcal{D}(\Omega)}$$

by considering the natural extension from $(0,L_z)$ to Ω (we recall that Ω is periodic in x and y):

$$\begin{array}{rccc} \tilde{\cdot} & : & \mathcal{D}(0,L_z) & \mapsto & \mathcal{D}(\Omega) \\ & & [z \mapsto v(z)] & \to & [z \mapsto \tilde{v}(x,y,z) = v(z)]. \end{array}$$

This process actually defines the averaging process with respect to x and y in the treatment of the source term. As a consequence, using the parametrization $s \mapsto \boldsymbol{\xi}(s,t)$ of the cilium

$$\begin{aligned} \left\langle \overline{f_x(\cdot,t)\delta_{\Gamma(t)}}^{x,y}, v \right\rangle_{\mathcal{D}'(0,L_z),\mathcal{D}(0,L_z)} &= \frac{1}{L_xL_y}\int_{\Gamma(t)} f_x((x,y,z);t)\,v(z)\,\mathrm{d}x\,\mathrm{d}y\,\mathrm{d}z \\ &= \frac{1}{L_xL_y}\int_0^L f_x(\boldsymbol{\xi}(s,t);t)\,v(\xi_z(s,t))\,|\nabla\boldsymbol{\xi}(s,t)|\,\mathrm{d}s \\ &= \frac{1}{L_xL_y}\int_0^L \hat{f}_x(s,t)\,v(\xi_z(s,t))\,|\nabla\boldsymbol{\xi}(s,t)|\,\mathrm{d}s. \end{aligned}$$

References

[1] S.K. Lai, Y.Y. Wang, D. Wirtz and J. Hanes. Micro- and macrorheology of mucus. *Adv. Drug Deliv. Rev.* **61** (2009) 86–100.

[2] M.R. Knowles and R.C. Boucher, Mucus clearance as a primary innate defense mechanism for mammalian airways. *J. Clin. Invest.* **109** (2002) 571–577.

[3] P.J. Basser, T.A. Mcmahon and P. Griffith, The mechanism of mucus clearance in cough. *Trans. ASME, J. Biomech. Eng.* **111** (1989) 288–297.

[4] A.M. Lucas and L.C. Douglas, Principles underlying ciliary activity in the respiratory tract: II. A comparison of nasal clearance in man, monkey and other mammals. *Arch. Otolaryngol.* **20** (1934) 518–541.

[5] I.R. Gibbons, Cilia and flagella of eukaryotes. *J. Cell. Biol.* **91** (1981) 107–124.

[6] D.R. Mitchell, The Evolution of Eukaryotic Cilia and Flagella as Motile and Sensory Organelles. Eukaryotic Membranes and Cytoskeleton: Origins and Evolution. Advances in Experimental Medicine and Biology, Vol. 607. Springer New York (2007) 130–140, chapter 11.

[7] N. Mizuno, M. Taschner, B.D. Engel and E. Lorentzen, Structural studies of ciliary components. *J. Mol. Biol.* **422** (2012) 163–180.

[8] B. Prevon, J.M. Scholey and E.J.G. Peterman, Intraflagellar transport: mechanisms of motor action, cooperation, and cargo delivery. *FEBS J.* **284** (2017) 2905–2931.

[9] E.M. Purcell, Life at low Reynolds number. *Am. J. Phys.* **45** (1977) 3–11.

[10] M.J. Sanderson and E.R. Dirksen, A versatile and quantitative computer-assisted photoelectronic technique used for the analysis of ciliary beat cycles. *Cell Motil.* **5** (1985) 267–292.

[11] D.R. Brumley, K.Y. Wan, M. Polin and R.E. Goldstein, Flagellar synchronization through direct hydrodynamic interactions. *eLife* **3** (2014) e02750.

[12] S. Enault, D. Lombardi, P. Poncet and M. Thiriet, Mucus dynamics subject to air and wall motion. *ESAIM: Proc.* **30** (2010) 125–141.

[13] S. Mitran, Continuum-kinetic-microscopic model of lung clearance due to core-annular fluid entrainment. *J. Comput. Phys.* **244** (2013) 193–211.

[14] B. Mauroy, C. Fausser, D. Pelca, J. Merckx and P. Flaud, Toward the modeling of mucus draining from the human lung: role of the geometry of the airway tree. *Phys. Biol.* **8** (2011) 056006, 12.

[15] D.J. Smith, E.A. Gaffney and J.R. Blake, A viscoelastic traction layer model of muco-ciliary transport. *Bull. Math. Biol.* **69** (2007) 289–327.

[16] P. Kurbatova, N. Bessonov, V. Volpert, H.A.W.M. Tiddens, C. Cornu, P. Nony and D. Caudri, Model of mucociliary clearance in cystic fibrosis lungs. *J. Theor. Biol.* **372** (2015) 81–88.

[17] A. Choudhury, M. Filoche, N.M. Ribe, N. Grenier and G.F. Dietze, On the role of viscoelasticity in mucociliary clearance: a hydrodynamic continuum approach. *J. Fluid Mech.* **971** (2023) A33.

[18] M. Bottier, M. Peña Fernández, G. Pelle, D. Isabey, B. Louis, J.B. Grotberg and M. Filoche, A new index for characterizing micro-bead motion in a flow induced by ciliary beating: Part II, modeling. *PLOS Comput. Biol.* **13** (2017) 1–21.

[19] A. Decoene, S. Martin and F. Vergnet, A continuum active structure model for the interaction of cilia with a viscous fluid. *Z. Angew. Math. Mech.* (2023) e202100534

[20] R.H. Dillon, L.J. Fauci, C. Omoto and X. Yang, Fluid dynamic models of flagellar and ciliary beating. *Ann. N. Y. Acad. Sci.* **1101** (2007) 494–505.

[21] S. Gueron and K. Levit-Gurevich, A three-dimensional model for ciliary motion based on the internal 9 + 2 structure. *Proc. Biol. Sci.* **268** (2001) 599–607.

[22] S. Gueron and N. Liron, Ciliary motion modeling, and dynamic multicilia interactions. *Biophys. J.* **63** (1992) 1045–1058.

[23] S. Gueron and N. Liron, Simulations of three-dimensional ciliary beats and cilia interactions. *Biophys. J.* **65** (1993) 499–507.

[24] M.H. Sedaghat, M.M. Shahmardan, M. Norouzi and M. Heydari, Effect of cilia beat frequency on muco-ciliary clearance. *J. Biomed. Phys. Eng.* **6** (2016) 265–278.

[25] M.H. Sedaghat, S. Sadrizadeh and O. Abouali, Three-dimensional simulation of mucociliary clearance under the ciliary abnormalities. *J. Non-Newton. Fluid Mech.* **316** (2023) 105029.

[26] S. Mitran, Metachronal wave formation in a model of pulmonary cilia. *Comput. Struct.* **85** (2007) 763–774.
[27] D. Oriola, H. Gadêlha and J. Casademunt, Nonlinear amplitude dynamics in flagellar beating. *R. Soc. Open Sci.* **4** (2017) 160698.
[28] Y. Man, F. Ling and E. Kanso, Cilia oscillations. *Philos. Trans. R. Soc. B* **375** (2019) 20190157.
[29] B. Chakrabarti and D. Saintillan, Hydrodynamic synchronization of spontaneously beating filaments. *Phys. Rev. Lett.* **123** (2019) 208101.
[30] B. Chakrabarti, S. Fürthauer and M.J. Shelley, A multiscale biophysical model gives quantized metachronal waves in a lattice of beating cilia. *Proc. Natl. Acad. Sci. U.S.A.* **119** (2022) e2113539119.
[31] R.G. Cox, The motion of long slender bodies in a viscous fluid. Part 1. General theory. *J. Fluid Mech.* **44** (1970) 791–810.
[32] Y. Mori, L. Ohm and D. Spirn, Theoretical justification and error analysis for slender body theory. *Commun. Pure Appl. Math.* **73** (2020) 1245–1314.
[33] N. Liron and S. Mochon, The discrete-cilia approach to propulsion of ciliated micro-organisms. *J. Fluid Mech.* **75** (1976) 593–607.
[34] G.R. Fulford and J.R. Blake, Force distribution along a slender body straddling an interface. *J. Austral. Math. Soc. Ser. B* **27** (1986) 295–315.
[35] D.J. Smith, E.A. Gaffney and J.R. Blake, Discrete cilia modelling with singularity distributions: application to the embryonic node and the airway surface liquid. *Bull. Math. Biol.* **69** (2007) 1477–1510.
[36] W.L. Lee, P.G. Jayathilake, Z. Tan, D.V. Le, H.P. Lee and B.C. Khoo, Muco-ciliary transport: effect of mucus viscosity, cilia beat frequency and cilia density. *Comput. Fluids* **49** (2011) 214–221.
[37] S. Chateau, J. Favier, U. D'Ortona and S. Poncet, Transport efficiency of metachronal waves in 3D cilium arrays immersed in a two-phase flow. *J. Fluid Mech.* **824** (2017) 931–961.
[38] R. Chatelin, Méthodes numériques pour l'écoulement de Stokes 3D: fluides à viscosité variable en géométrie complexe mobile ; application aux fluides biologiques. *Thèse de doctorat de l'université Paul Sabatier* (2013) 197.
[39] O.K. Matar and P.D.M. Spelt, Dynamics of thin free films with reaction-driven density and viscosity variations. *Phys. Fluids* **17** (2005) 122102.
[40] S. Bertoluzza, A. Decoene, L. Lacouture and S. Martin, Local error analysis for the Stokes equations with a punctual source term. *Numer. Math.* **140** (2018) 677–701.
[41] L. Lacouture, Modélisation et simulation du mouvement de structures fines dans un fluide visqueux : application au transport mucociliaire. *Thèse de doctorat de l'université Paris-Sud* (2016).
[42] G.R. Fulford and J.R. Blake, Muco-ciliary transport in the lung. *J. Theor. Biol.* **121** (1986) 381–402.
[43] M.J. Sanderson and M.A. Sleigh, Ciliary activity of cultured rabbit tracheal epithelium: beat pattern and metachrony. *J. Cell Sci.* **47** (1981) 331–347.
[44] L. Gheber, A. Korngreen and Z. Priel, Effect of viscosity on metachrony in mucus propelling cilia. *Cell Motil. Cytoskel.* **39** (1998) 9–20.
[45] T.L. Hayden, Representation theorems in reflexive Banach spaces. *Math. Z.* **104** (1968) 405–406.
[46] C.G. Simader, On Dirichlet's Boundary value Problem. An L^p-theory based on a generalization of Garding's inequality. Vol. 268 of *Lecture Notes in Mathematics*. Springer-Verlag, Berlin-Heidelberg-New York (1972).
[47] F. Hecht, New development in freefem++. *J. Numer. Math.* **20** (2012) 251–265.
[48] W.M. Foster, E. Langenback and E.H. Bergofsky, Measurement of tracheal and bronchial mucus velocities in man: relation to lung clearance. *J. Appl. Physiol.* **48** (1980) 965–971.
[49] E. Kilgour, N. Rankin, S. Ryan and P. Rodger, Mucociliary function deteriorates in the clinical range of inspired air temperature and humidity. *Intensive Care Med.* **30** (2004) 1491–1494.
[50] D.B. Yeates, N. Aspin, H. Levison, M.T. Jones and A.C. Bryan, Mucociliary tracheal transport rates in man. *J. Appl. Physiol.* **39** (1975) 487–495.
[51] R. Trawoger, T. Kolobow, M. Cereda and M.E. Sparacino, Tracheal mucus velocity remains normal in healthy sheep intubated with a new endotracheal tube with a novel laryngeal seal. *Anesthesiology* **86** (1997) 1140–1144.
[52] L. Morgan, M. Pearson, R. de Iongh, D. Mackey, H. van der Wall, M. Peters and J. Rutland, Scintigraphic measurement of tracheal mucus velocity in vivo. *Eur. Respir. J.* **23** (2004) 518–522.
[53] A. Decoene, S. Martin and B. Maury, Direct simulation of rigid particles in a viscoelastic fluid. *J. Non-Newton. Fluid Mech.* **260** (2018) 1–25.